A&A 403, Online Material (2003)

Astronomy & Astrophysics

Explanatory Supplement of the ISOGAL-DENIS Point Source Catalogue ⋆,⋆⋆

F. Schuller[1], S. Ganesh[2,1], M. Messineo[3], A. Moneti[1], J.A.D.L. Blommaert[4], C. Alard[1,5], B. Aracil[1], M.-A. Miville-Deschênes[6], A. Omont[1], M. Schultheis[1], G. Simon[5], A. Soive[1], and L. Testi[7]

[1] Institut d'Astrophysique de Paris, CNRS, 98 bis Bd Arago, F-75014 Paris, France
[2] Physical Research Laboratory, Navarangpura, Ahmedabad 380009, India
[3] Leiden Observatory, University of Leiden, P.O. Box 9513, 2300 RA Leiden, The Netherlands
[4] Instituut voor Sterrenkunde, K. U. Leuven, Celestijnenlaan 200 B, B-3001 Leuven, Belgium
[5] GEPI, Observatoire de Paris, 61, av. de l'Observatoire, F-75014 Paris, France
[6] Laboratoire de radioastronomie millimétrique, Ecole Normale Supérieure & Observatoire de Paris, France
[7] Osservatorio Astrofisico di Arcetri, Largo E. Fermi, 5, 50125 Firenze, Italy

Abstract. We present version 1.0 of the ISOGAL–DENIS Point Source Catalogue (PSC), containing more than 100,000 point sources detected at 7 and/or 15 μm in the ISOGAL survey of the inner Galaxy with the ISOCAM instrument on board the *Infrared Space Observatory* (ISO). These sources are cross-identified, wherever possible, with near-infrared (0.8—2.2 μm) data from the *DENIS* survey. The overall surface covered by the ISOGAL survey is about 16 square degrees, mostly (95%) distributed near the Galactic plane ($|b| \lesssim 1^\circ$), where the source extraction can become confusion limited and perturbed by the high background emission. Therefore, special care has been taken aimed at limiting the photometric error to ~ 0.2 magnitude down to a sensitivity limit of typically 10 mJy. The present paper gives a complete description of the entries and the information which can be found in this catalogue, as well as a detailed discussion of the data processing and the quality checks which have been completed. The catalogue is available via the VizieR Service at the Centre de Données Astronomiques de Strasbourg (CDS, http://vizier.u-strasbg.fr/viz-bin/VizieR/) and also via the server at the Institut d'Astrophysique de Paris (http://www-isogal.iap.fr/).

Key words. Catalogs – Stars: circumstellar matter – Galaxy: bulge – Galaxy: disk – Galaxy: stellar content – Infrared: stars

Contents

Note: Figures present only in this electronic version of the paper are labelled with an E- in front of their number.

Send offprint requests to: F. Schuller, schuller@iap.fr

⋆ This is paper no. 18 in a refereed journal based on data from the ISOGAL project

⋆⋆ Based on observations with ISO, an ESA project with instruments funded by ESA Member States (especially the PI countries: France, Germany, the Netherlands and the United Kingdom) and with the participation of ISAS and NASA; and on DENIS observations collected at the European Southern Observatory, Chile

1. Introduction

The ISOGAL survey is the most sensitive mid-infrared wide-field survey dedicated to the inner Galaxy (see the accompanying paper Omont et al. 2003 and references therein for a review of its scientific goals and results). The large amount of ISO observations collected, in combination with the near-infrared data of the DENIS survey, has resulted in the production of a catalogue of 10^5 point sources, the PSC. The first scientific results obtained include studies of the Galactic structure, analysis of the stellar populations comprising completely detected AGB stars with their mass-loss in particular fields (Pérault et al. 1996; Omont et al. 1999; Glass et al. 1999; Ojha et al. 2003), characterisation of interstellar extinction (Jiang et al. 2003), of infrared dark clouds (Hennebelle et al. 2001), and of young stellar objects (Felli et al. 2000 and 2002; Schuller 2002).

A total of ∼16 square degrees of the inner Galactic disk ($|b| \lesssim 1°$) were observed, with strong emphasis on the inner Galactic bulge, at wavelengths of 7 and 15 μm, with a pixel scale of usually 6" and sometimes 3", down to a sensitivity limit of typically 10 mJy. A total of ~ 250 hours of ISO time were used, making ISOGAL one of the largest programs performed by ISO. For the southern sky the results were combined with the I, J, K_s (effective wavelengths equal to 0.79, 1.22 and 2.14 μm) ground-based data from the DENIS survey (Epchtein et al. 1994, 1997) in order to produce an (up to) 5-wavelength catalogue of point sources. Given the emphasis of ISOGAL on the inner Galactic regions, the DENIS coverage is available for 95% of the fields surveyed with ISOCAM.

As a comparison, the IRAS satellite, which made a breakthrough in the infrared window in 1983, performed an all sky survey resulting in a 2.5×10^5 point source catalogue, with a typical sensitivity (or 90% completeness level) around 0.5 Jy in low source density regions and at the shortest wavelengths. The four IRAS bands were centred at 12, 25, 60 and 100 μm, thus covering the mid- to far-infrared range, with a spatial resolution ranging from less than 1' at 12 μm to about 4' at 100 μm. The sensitivity of ISOCAM is about two orders of magnitude better than that provided by the IRAS detectors at 12 μm in the high source density regions (thus in particular in the Galactic plane). Indeed, as explained in the IRAS Explanatory Supplement (Section VIII), the typical 50% completeness limit flux density was about 1 Jy at 12 and 25 μm in the Galactic Plane, and even brighter at longer wavelengths.

More recently, the MSX (Midcourse Space Experiment, see Mill et al. 1994 for an overview) mission surveyed the complete Galactic Disk in the range $|b| \leq 5°$ in the mid-infrared, using a 33 cm aperture telescope called SPIRIT III (Price et al. 2001). Six bands between 4 and 25 μm were surveyed simultaneously at a spatial resolution of $\sim$ 18". The most sensitive band was the A band, centred at 8.3 μm, for which the present point source sensitivity limit is about 0.1 Jy. The survey of the Galactic Plane has presently resulted in a catalogue of 3.2×10^5 sources (Price et al. 2001), which permits a complete analysis of the most luminous infrared Galactic populations. The images of this survey have also led to the detection of more than 2000 infrared dark clouds (Egan et al. 1998). A very recent analysis (Lumsden et al. 2002) of the MSX PSC has produced a large sample of massive young stellar objects in the Galactic disk.

Among the many large observing programs conducted by ISO, including deep and wide-field extragalactic surveys, worth mentioning are the European Large-Area ISO Survey, ELAIS (Rowan-Robinson et al. 1999), ISOCAM deep surveys using guaranteed time observations (Elbaz et al. 1999), and FIRBACK, a deep 170 μm imaging survey carried out with ISOPHOT (Dole et al. 2001). Apart from these there were also a number of observations of specific targets in the Galaxy. The following ISOCAM studies were with sensitivities comparable to or slightly deeper than ISOGAL (in more limited areas): LW2 and LW3 imaging surveys of nearby star forming regions (Nordh et al. 1998; Bontemps et al. 2001), photometric studies of other Galactic HII regions (Zavagno & Ducci 2001), and the GPSURVEY (Burgdorf et al. 2000), which provided observations of about 0.25 deg^2 in the central Galaxy at mid-infrared wavelengths.

In this paper, we give a detailed description of the ISOGAL observations in Sect. 2, and of their processing and the related quality checks in Sect. 3. The DENIS data are presented in Sect. 4. The content of the Point Source Catalogue (PSC) is explained in Sect. 5, and the complete descriptions of various support tables are given in the relevant sections. Finally, the main characteristics of the catalogue are briefly summarised in Sect. 8.

2. ISOGAL Observations and Fields

2.1. ISOGAL observations

The mid-infrared observations were obtained with the ISOCAM instrument (Cesarsky et al. 1996; Blommaert et al. 2001) on ISO (Kessler et al. 1996) using filters centred at $\lambda \approx 7$ and 15 μm and with a pixel scale of 6", or 3" in a few cases. Table 1 lists the filters used.

Table 1. ISOCAM filters used for ISOGAL: reference wavelengths and bandwidths, zero point magnitudes and flux densities, and total observed area.

Filter	λ_{ref} [μm]	$\Delta\lambda$ [μm]	ZP[a] [mag]	$F_{mag=0}$ [Jy]	Area [deg^2]
LW2	6.7	3.5	12.39	90.36	9.17
LW5	6.8	0.5	12.28	81.66	0.64
LW6	7.7	1.5	12.02	64.27	2.97
LW3	14.3	6.0	10.74	19.77	9.92
LW9	14.9	2.0	10.62	17.70	3.53

[a] The magnitude of a source with a flux density F_ν expressed in mJy is given by $mag = ZP - 2.5 \times log(F_\nu)$

Most observations were performed with the broad filters LW2 and LW3, with a field selection avoiding bright IRAS sources susceptible to detector array saturation. However, a few regions with stronger sources (around the Galactic Centre and in a few star forming regions) were observed with the narrow filters LW5 or LW6, and LW9, and with smaller pixel field of view (3").

For standard ISOGAL observations (broad filters LW2 and LW3), we estimated that, to avoid saturation of the detector, no IRAS source with $F_{12\mu m} \geq 6$ Jy should be observed. This limit was further relaxed up to $F_{12\mu m} < 20$ Jy with narrow filters; however, even with such a high limit value, it implied that a few regions, including the Galactic Centre itself, could not be observed. A quick inspection of the images showed that only very few observed pixels among all ISOGAL observations were slightly above the limit of the linear domain of the detector. The profiles of the associated point sources do not deviate much from the average point spread function (PSF, see Sect. 3.2.1), so that no source suffers strongly from saturation in the published point source catalogue.

The observations were performed as rasters. The basic ISOCAM observation is a 32×32 pixel image of 0.28 sec integration time. Due to limitations in the downlink data rate, these basic images were coadded in groups of four and downlinked, making the unit frame one of 1.12 sec integration time. At each raster position 19 such frames were obtained, resulting in an integration time of ~ 21 sec per raster position. The rasters were oriented along galactic latitude and longitude, which differed from the direction of the sides of the detector array, resulting in "saw-tooth" edges of the final mosaics. With 6" pixels, the raster steps were typically 90" in one direction and 150" in the perpendicular one (and a factor of two smaller with 3" pixels), in order to observe each sky position about twice. However, because of the non-alignment of the raster and detector axes, each sky position was not as regularly observed. The actual number of observations per sky point varied from four to exceptionally zero (for the dead ISOCAM column close to a raster edge), with an average of ~ 1.5.

The total area covered by the ISOGAL survey is ~ 15.6 square degrees, of which 10.7 were observed at both 7 and 15 μm, 2.1 were observed at 7 μm only, and 2.8 were observed at 15 μm only. This survey is the result of three successive proposals developed over the lifetime of the ISO satellite. As a consequence, most fields were observed at 7 and 15 μm at different dates, and some fields were observed at one wavelength only, in particular because the planned targets were not observable at the very end of the mission.

A total of 696 observations compose the ISOGAL survey. Of all these observations, 29 could not be used because of instrument failures or other problems during the data reduction. Another 18 observations are single ISOCAM frames (32x32 pixels) observed in the spectroscopic *Circular Variable Filter* (CVF) mode; they are treated in a different way (Blommaert et al., in preparation). A further 186 images are "dummy" observations, containing only one 32×32 pixel image - acquired after repositioning of the telescope to allow for reconfiguring the camera from the CAM parallel mode to that of the observation - and have not been used for the catalogue. As a result, only 463 raster-observations are considered as relevant for the imaging survey.

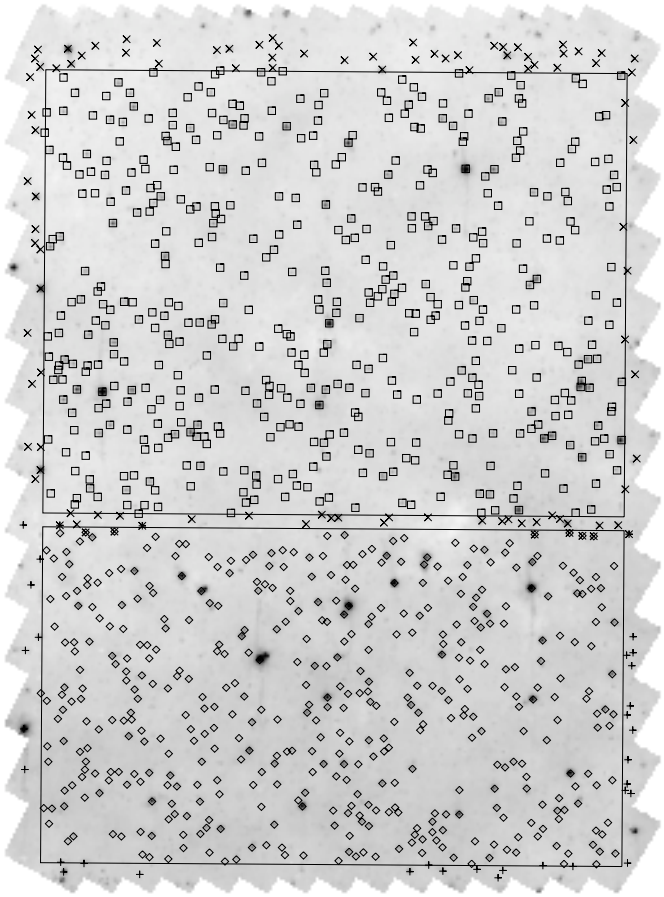

Fig. 1. Example of one ISOGAL observation which has been used for one FA and one FC fields. The formal limits of both fields are shown with rectangular frames: FC field (upper frame) and FA field (lower frame). The different symbols correspond to the different catalogues of sources (see Sect. 5): squares (FC, regular), crosses (FC, edge), diamonds (FA, regular) and plus signs (FA, edge).

To avoid redundancy in the published catalogue (due e.g. to various observations of a test field with several filters, but also to small overlapping areas between two observations in many cases), we decided to use, for the present version of the PSC, only one observation at 7 μm and one at 15 μm for a given position[1]. Thus, we had to choose the best observation in the case of overlapping images at the same wavelength. The selection criteria were: first, if the different observations are obviously of different quality, the best quality one was selected. Then, if the

[1] However, in very few cases due to edge effects, two ISOGAL sources have exactly the same final coordinates because they are associated with the same DENIS source (see also Sect. 5)

Table 2. Format of ISOGAL Observations Table (version 1) - 384 entries (see examples in Table 3)

Col.	Name	Format	Units [range]	Description
1	ION	a8		ISO Observation number
2	name	a13		ISOGAL observation name
3	date	a6	YYMMDD	date of observation
4	j_day	i4		Julian day of observation - 2450000
5	qual	i1	[1,2]	quality of image[a]
6	l_off	f5.1	arcsec	applied offset in Galactic longitude[b]
7	b_off	f5.1	arcsec	applied offset in Galactic latitude
8	G_lon	f8.4	deg [-180–+180]	Galactic longitude of raster centre
9	G_lat	f8.4	deg [-90–+90]	Galactic latitude of raster centre
10	dl	f6.4	deg	half width of raster in longitude
11	db	f6.4	deg	half width of raster in latitude
12	RA	f8.4	deg	RA (J2000) of raster centre
13	DEC	f8.4	deg	Dec (J2000) of raster centre
14	filt	i1	[2,3,5,6,9]	LW filter number
15	pfov	i1	arcsec [3,6]	pixel field of view
16	mag_lim	f5.2	mag	ISO magnitude cutoff[c]
17	nb_sour	i4		number of extracted sources brighter than mag_lim
18	rot	i1	[0,1]	applied transformation (270° rotation) to the raster[d]
19	x_inv	i1	[0,1]	applied transformation (x-inversion) to the raster
20	y_inv	i1	[0,1]	applied transformation (y-inversion) to the raster
21	m	i2		number of raster steps in x in final raster
22	n	i2		number of raster steps in y in final raster
23	dm	i3	arcsec	size of step between x (final) raster positions
24	dn	i3	arcsec	size of step between y (final) raster positions
25	angle	f6.2	deg	angle from the upward axis to the north in the final raster
26	NX	i3	pixel	number of pixels in x of final raster
27	NY	i3	pixel	number of pixels in y of final raster

[a] Image quality: 1 is standard quality, 2 is medium quality (in most cases, the problem is that the first individual image of the raster appears brighter than the other ones). Images of bad quality have not been used to build the catalogue.

[b] The astrometry of the published raster images has been corrected to match the DENIS astrometry if any (see Sect. 7). The offset values given in this table have been added to the initial raster coordinates.

[c] The ISO magnitude cutoff has been computed for each observation to correspond at least approximately to a 50% completeness level (see Sect. 3.4).

[d] Cols. 18, 19 and 20: all the published images are oriented with l along decreasing x and b along increasing y. In each column, a 1 means that the corresponding transformation has been applied to the initial (OLP7 processed) raster, and a 0 means that this transformation was not needed.

observations were made with different filters, we chose to keep the one with a broad filter (if it exists) because the number of detected sources is larger. In the very few cases where the filter is the same but the pixel size is different, we selected the large (6") pixel observations in order to have more homogeneous data. If the quality and the observational setup were approximately the same in different observations, we then selected the most recent one (the one with higher ISO observation number), because on average the data quality was better certified. Finally, 384 raster images have been used to build the PSC.

All the raster images used are published with the PSC (and available through the CDS and IAP web sites[2]), and the electronic version of the Catalogue of ISOGAL Observations of the PSC contains 384 entries, each entry having the format described in Table 2. Two examples are shown in Table 3, for the 7 and 15 μm observations composing a test field of 0.027 deg^2 centred at $(l, b) = (0.0, 1.0)$, hereafter called the "C32" field.

2.2. Definition and list of "Catalogue Fields"

We define an ISOGAL "field" as a rectangular area of the sky whose edges are aligned with the galactic axes, and which has been completely observed with ISOCAM. There are three kinds of fields, depending on the available observations: the "FA" fields were observed only at 7 μm, the "FB" fields were observed only at 15 μm, and the "FC" fields were observed at both 7 μm and 15 μm.

To build the present version of the PSC, we have defined a total of 43 FA fields, 57 FB fields and 163 FC fields. In some cases, a fraction of an ISOGAL observation was

[2] http://www-isogal.iap.fr/Fields/index_tdt.html

Table 3. Two examples of entry in the ISOGAL Observations Table (see Table 2 for explanation), from the "C32" field at $(l, b) = (0.0, 1.0)$

Col.	Name	Example 1	Example 2	Col.	Name	Example 1	Example 2
1	ION	83600418	83600523	14	filt	2	3
2	name	2P00P10B	3P00P10B	15	pfov	6	6
3	date	980228	980228	16	mag_lim	8.89	8.00
4	j_day	873	873	17	nb_sour	331	220
5	qual	1	1	18	rot	1	1
6	l_off	-4.8	-6.3	19	x_inv	0	0
7	b_off	-5.6	-3.1	20	y_inv	0	0
8	G_lon	0.0001	-0.0003	21	m	7	7
9	G_lat	0.9988	0.9995	22	n	4	4
10	dl	0.1633	0.1633	23	dm	150	150
11	db	0.0758	0.0758	24	dn	90	90
12	RA	265.4353	265.4343	25	angle	58.95	58.97
13	DEC	-28.4136	-28.4136	26	NX	196	196
				27	NY	91	91

Table 4. Format of ISOGAL "Fields" Table (version 1) - 263 entries (see example in Table 5)

Col.	Name	Format	Units [range]	Description
1	Name	a14		ISOGAL field identifier
2	ION7	a8		ION for 7 μm data (see Table 2)
3	ION15	a8		ION for 15 μm data
4	filt7	i1	[2,5,6]	7 μm filter
5	filt15	i1	[3,9]	15 μm filter
6	pfov	i1	arcsec [3,6]	pixel field of view
7	G_lon	f8.4	deg [-180–+180]	Galactic longitude of field centre
8	G_lat	f8.4	deg [-90–+90]	Galactic latitude of field centre
9	dl	f6.4	deg	half width of field in longitude[a]
10	db	f6.4	deg	half width of field in latitude[a]
11	area	f6.4	deg^2	area of field
12	dens7	i5	deg^{-2}	density of 7 μm sources
13	dens15	i5	deg^{-2}	density of 15 μm sources
14	RMS_II	f4.2	arcsec	RMS separation of 7-15 μm associated sources
15	RMS_ID	f4.2	arcsec	RMS separation of ISO-DENIS associated sources
16	K_max1	f4.1	mag	DENIS K_s magnitude cutoff 1[b]
17	K_max2	f4.1	mag	DENIS K_s magnitude cutoff 2[c]
18	dens_K2	i5	deg^{-2}	density of DENIS K_s sources used[d]

[a] *dl* and *db* apply to the limits inside the edges of the images within which sources are accepted.

[b] maximum DENIS K_s magnitude limiting the density of K_s DENIS sources to $\sim$ 18 000 sources per square degree if the ISO images have 6" pixels (or to $\sim$ 72 000 sources per square degree for the 3" ISO observations). K_max1 is used to discuss the quality of ISOGAL–DENIS associations (see Sect. 4.4.5).

[c] maximum DENIS K_s magnitude accepted in order to avoid spurious cross-identifications. The density of K_s DENIS sources is limited to $\sim$ 36 000 sources per square degree for 6" ISO observations (and again to $\sim$ 72 000 sources per square degree for 3" ISO observations).

[d] density of DENIS K_s-band sources brighter than the cutoff magnitude K_max2.

used for an FA (or FB) field, and another fraction was used for an FC field (see e.g. Fig. 1), so that only 384 different observations were required for these 263 fields. These peculiar configurations can result in the presence of a few redundant sources: because of edge effects, two sources at the same position may appear in two different catalogues; nine such cases can be seen on Fig. 1 (see also Sect. 5.1).

The complete catalogue of the 263 ISOGAL fields is available electronically[3] and contains 18 columns, as described in Table 4, and an example is given in Table 5.

[3] http://www-isogal.iap.fr/Fields/ and from the VizieR service at CDS: http://vizier.u-strasbg.fr/viz-bin/VizieR

Table 5. Example of entry in the ISOGAL Fields Table (Table 4) ("C32" field at $(l, b) = (0.0, 1.0)$)

Col.	Name	C32 field
1	Name	FC+00000+00100
2	ION7	83600418
3	ION15	83600523
4	filt7	2
5	filt15	3
6	pfov	6
7	G_lon	-0.0011
8	G_lat	0.9990
9	dl	0.1441
10	db	0.0471
11	area	0.0271
12	dens7	9225
13	dens15	6125
14	RMS_II	2.24
15	RMS_ID	1.70
16	K_max1	9.6
17	K_max2	10.6
18	dens_K2	35979

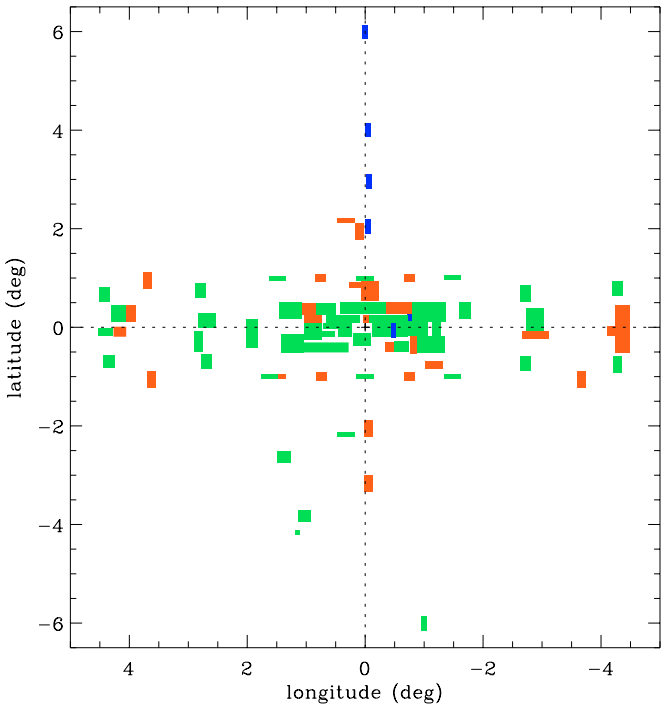

Fig. E-2. Galactic map of the ISOGAL "bulge" fields. The green boxes show the fields which have been observed at both 7 and 15 μm (FC fields), while the blue boxes stand for 7 μm only observations (FA), and the red ones for 15 μm only observations (FB). The cross shows the position of the Galactic Centre.

The field names are generated using 14 characters, and the first two indicate the type of the field (FA, FB or FC). The 12 last characters of the field names are the galactic coordinates in decimal degrees of the centre of the field. The complete list of fields is given in the appendix, with only the first ten columns (name, ISO observations numbers, filters and pixel size, coordinates and size). Graphical views of the observed fields are given in Fig. E-2 and Fig. 3.

3. ISOGAL data processing and quality

3.1. ISOCAM image processing

Data reduction was performed with the CAM Interactive Analysis (CIA, Ott et al. 1997) package version 3.0 on data products produced with version 7.0 of the ISO Off-Line Processing (OLP) pipeline (Blommaert et al. 2001). Starting with the SPD (science processed data) files we proceeded with the following steps: first, the dark correction is applied using the default method of model dark as described in Biviano et al. (1998). The data cube is then deglitched (removal of cosmic ray hits) using the "multi-resolution median" method. The transient behaviour of the detector is stabilised next using the IAS model transient correction (Abergel et al. 1998), also called the 'inversion' method for transient correction.

The difficulty in reducing ISOCAM data stems from the slow response of the detectors to changes in input flux and, specifically, from the fact that, for the ISOGAL survey, the measurement was too short to allow the signal to reach a stabilised value. This produced two side-effects: when a source appears on a pixel, the measured signal is lower than the true signal, and when a source is removed from a pixel, a latent image (or remnant) of the source remains (Coulais & Abergel 2000). Indeed, the detector response to a strong downward step in flux can last more than one minute, which is long in comparison with the typical integration time per position ($\sim$ 21 sec) and with the time needed to move from one position to the next one in a raster (typically 10 sec).

Therefore, on a copy of the deglitched data we also run the 'vision' method (Starck 1998; Starck et al. 1998) of treating the memory remnant effect of the ISOCAM detector pixels. This method does not correct for the transients but eliminates most of the spurious sources that are present in the data due to the pixel memory. We thus have at this stage onwards two sets of data - one treated with 'vision', where remnants have been removed, and one with 'inversion', which performs a correction for the missing signal, thus giving a better estimate of the source signal (but this correction is not perfect, see Sect. 3.3.1), but which still contains the remnants.

Next, the different detector readouts at the same satellite pointing are averaged, and the average image of each pointing is flat fielded using a flat field generated from the data themselves, by taking a median image over all individual frames in the raster. Tests made on the C32 test field (LW2 filter, 3" and 6" pixels observations with 'inversion' transient correction) with flats generated from the data and from the flat field library do not show any

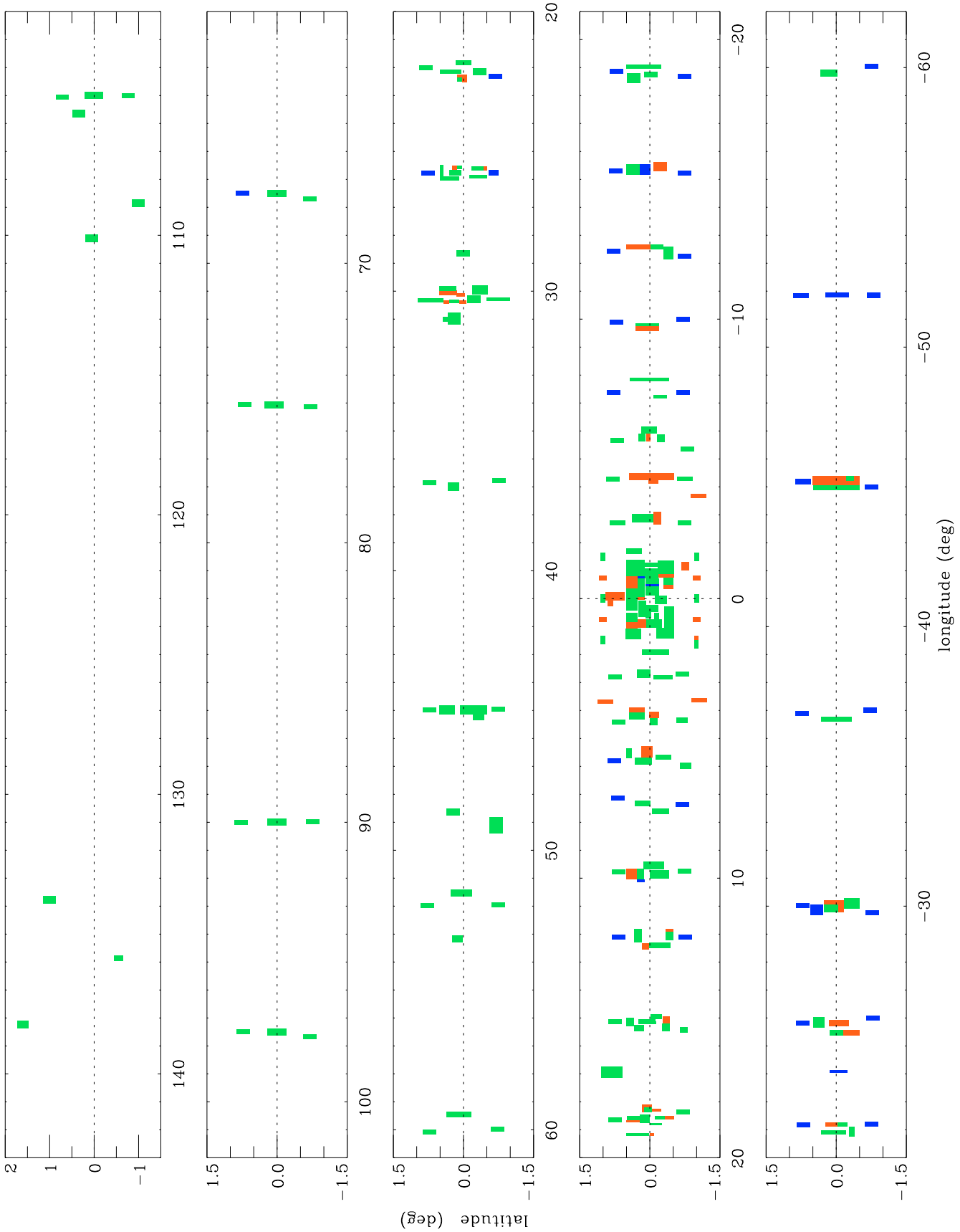

Fig. 3. Galactic map of the ISOGAL disk fields. Same symbols as in Fig. E-2.

significant difference over the usual photometric noise. After flat fielding, the individual images are corrected for field of view distortions using Aussel's (1998) distortion matrices and then mosaiced. The two rasters (treated with 'vision' and 'inversion') are then converted to physical units (mJy), using the standard conversion factors (Blommaert 1998). This ISOCAM data reduction process is summarised in Fig. E-4.

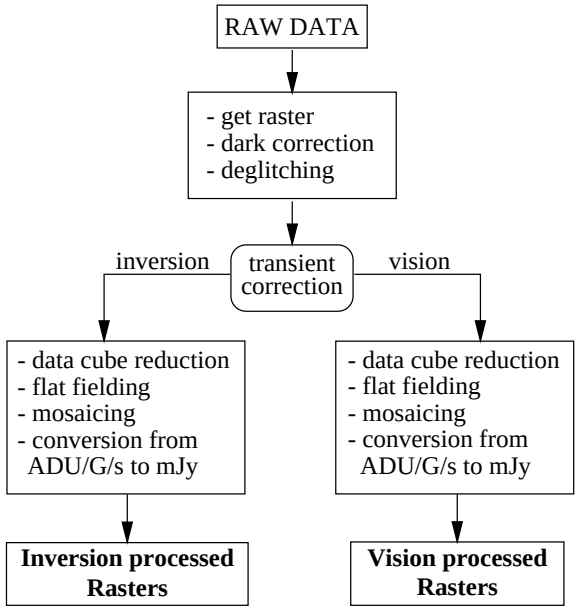

Fig. E-4. Summary of the ISOCAM image processing before source extraction. The processing was done on products produced by OLP7 and using calibration files of that version.

3.2. Point source extraction

A dedicated PSF fitting procedure worked out by C. Alard has been used to extract point sources from all 'inversion' and 'vision' processed images. First, a search for local maxima is performed on the complete image, resulting in a list of pixel positions of point source candidates. Then, an analytical expression of the PSF is fitted at each position to compute the flux density of the point sources, and to discard the local maxima whose shapes do not correspond to the instrumental response to a point source.

3.2.1. Determination of the PSF

The measurement of the flux density is performed with a PSF fitting algorithm. For each observational setup (combination of one filter and one pixel size), a reference PSF has first been extracted from a subsample of good quality raster images. Typically five to ten images without obvious defects and with moderate source density and no bright extended object have been selected for each setup. Then, a large number (between 10 and 50 for each setup) of bright sources were selected, and a PSF was determined for each source. This PSF is defined by the following analytical expression:

$$F(r) = C_1 \times e^{-3Wr^2} + C_2 \times e^{-Wr^2} + C_3 \times e^{-Wr^2/3} \quad (1)$$

where C_1, C_2, C_3 and W result from the resolution of a linear system, using a 5×5 pixel sample of the image. Finally, all the resulting PSF profiles were plotted, and the ones which clearly deviate from the mean distribution were discarded. Then, the coefficients of the reference PSF were defined by the normalised median values of the coefficients found for the remaining sources. The normalisation is done so that:

$$\int_0^{2\pi} \int_0^{+\infty} F(r)\, r\, dr\, d\theta = 1$$

which is equivalent to:

$$\frac{C_1\,\pi}{3\,W} + \frac{C_2\,\pi}{W} + \frac{3\,C_3\,\pi}{W} = 1$$

The profiles of the reference PSFs that we derived by this method for the different observational setups are plotted in Fig. E-5, and the corresponding coefficients C_1, C_2, C_3 and W are given in Table 6.

Table 6. Coefficients of the analytical expression of the PSF for the different observational setups (see Eq. (1)).

Filt.	Pixel	W	C_1	C_2	C_3
LW2	3"	0.757	0.160	0.094	0.031
LW5	3"	0.759	0.136	0.118	0.026
LW6	3"	0.694	0.162	0.107	0.020
LW3	3"	0.648	0.087	0.108	0.023
LW9	3"	0.675	0.065	0.131	0.021
LW2	6"	1.307	0.130	0.311	0.021
LW5	6"	1.231	0.145	0.312	0.013
LW6	6"	1.409	0.078	0.370	0.019
LW3	6"	1.147	0.149	0.213	0.034
LW9	6"	0.969	0.191	0.163	0.036

3.2.2. Detection of the point source candidates

The source detection procedure first computes an oversampled image using pixels a factor of two smaller than in the initial image. This image is used only for the detection step of the source extraction. The oversampling is performed by a convolution of the initial pixels with an analytical expression of a theoretical PSF. As a result, the sources can be localised on a thinner grid.

Then the procedure looks for local maxima in the oversampled image. This step is controlled by a *mesh* parameter, which can take values of 1 or 2, and defines the size of the grid on which local maxima are looked for. A pixel position (x, y) in the oversampled image is considered as a source candidate if its flux density is the maximum value in the range $([x - mesh, x + mesh], [y - mesh, y + mesh])$,

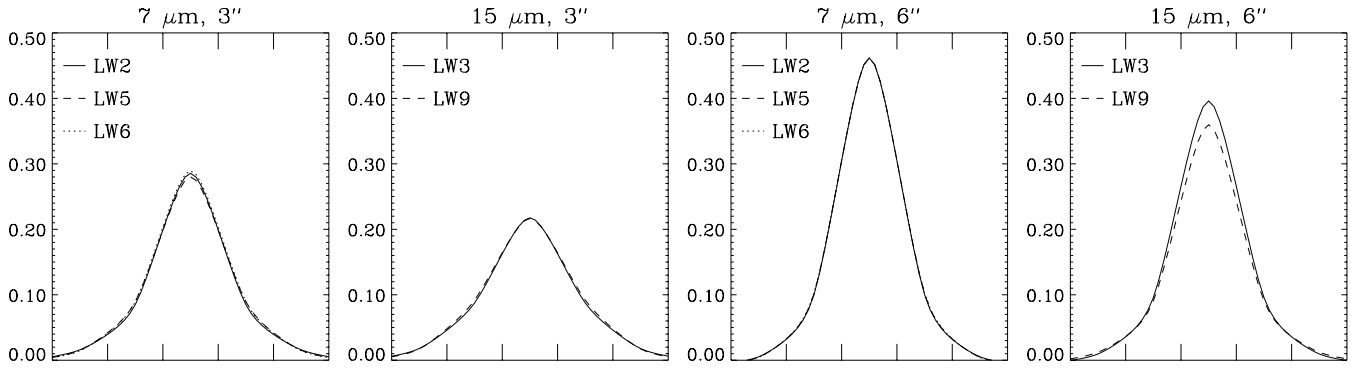

Fig. E-5. Profiles of all used reference PSFs. The graduations on the abscissa axis correspond to pixels. The different line styles correspond to the different filters, as shown in the upper left corner of each panel.

i.e. in a 3×3 oversampled pixels sample for $mesh = 1$ and 5×5 pixels for $mesh = 2$. Therefore, with $mesh = 1$, all local maxima are detected, even those corresponding to bright spots in the background rather than to point sources. They are nevertheless eliminated during the next step of the extraction procedure if their profile clearly deviates from the PSF (namely when the ratio of the flux density to the RMS uncertainty is less than 3, see next paragraph). On the other hand, with $mesh = 2$, 5×5 oversampled pixel meshes are used to find local maxima, resulting in a smoothing of the irregularities in the background, without any significant loss in the detection of relatively bright ($F_\nu \gtrsim 100$ mJy) point sources, but with a more confusion limited extraction of the faintest sources.

The extraction procedure which has been used to build the ISOGAL PSC performed a complete extraction with each value of *mesh*. For each observation, the two resulting catalogues have been cross associated to check the quality and the reality of the detected sources (see Sect. 3.2.4). Obviously the extraction performed with $mesh = 1$ is the most efficient to correctly extract blended sources; on the other hand, a non negligible fraction of the sources extracted only with $mesh = 1$ (with no association in the extraction performed with $mesh = 2$) seem to be spurious (see the discussion in Sect. 3.5.3).

3.2.3. PSF photometry

The list of positions of the detected sources is passed to another procedure whose purpose is to measure the flux density of the sources on the original image, and to estimate the correlation with the PSF. A least square fit between the reference profile and a 5×5 (not oversampled) pixel mesh is computed at each position, starting with the brightest source. The background is estimated from the median value of the pixels in an annulus of inner and outer radii equal to 3 and 5 pixels, respectively. The results of this operation are the flux density of the source and the uncertainty on its measurement, computed as the RMS of the residual between the scaled PSF profile and the actual source profile. This flux density uncertainty is later converted to a magnitude uncertainty, hereafter called σ.

The reality of each point source is estimated by the ratio of the fitted flux density to the RMS uncertainty of the fit, and only sources with this ratio greater than 3 are considered valid and stored in the resulting catalogue. Then, the profile of the source is subtracted from the image, and the procedure runs iteratively going to fainter and fainter sources. This method is powerful even in crowded fields, where it is able to estimate correctly the flux densities of blended sources.

3.2.4. Source quality checks

Four catalogues have been built for each observation, combining the two possible values of *mesh* (1 or 2) and the 'inversion' and 'vision' processed rasters. Considering the high background level in the Galactic Disk, we decided to anyhow limit the published catalogue to a flux density of 5 mJy ([7]≈10.5 and [15]≈9.0) to reduce the number of spurious sources (another limit was eventually later applied depending on the field, see Sect. 3.4.5). The catalogues extracted from the 'inversion' rasters were limited to 5 mJy at this processing stage, while this cut was relaxed to 2.5 mJy for the 'vision' catalogues, because the latter tend to underestimate fluxes of real sources, making a source appear fainter than in the 'inversion' raster.

Then, the sources found in 'inversion' processed images that were associated with a 'vision' source within a search radius of one observed pixel were considered valid, while those found only in the 'inversion' images were considered spurious (these can be remnants of bright sources, or other non real point-like sources). The distance between the 'inversion' and the 'vision' sources gives a good estimate of the quality of the sources: it is generally smaller than 1" for real sources, while a separation larger than 3" may be due to artifacts (see also Sect. 3.2.8). The final data (position and photometry) in the catalogue come only from the 'inversion' processed rasters, with elimination of the remnant sources using the 'vision' results.

The majority (70%) of the extracted sources could be associated between the $mesh = 1$ and the $mesh = 2$ catalogues (with a 6" association radius for all observations), while the remaining 30% are only found with $mesh = 1$.

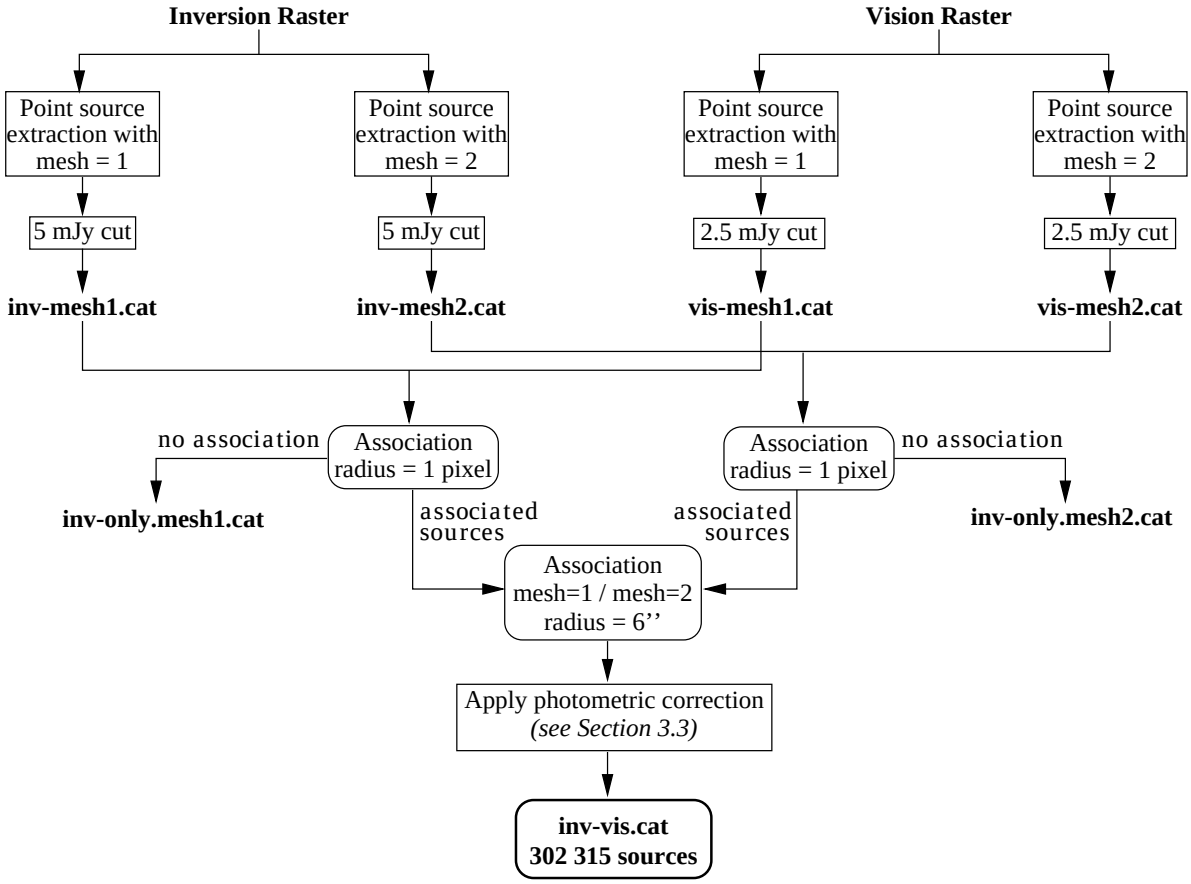

Fig. E-6. Summary of the first steps of the point source extraction.

This sequence of extraction and association processes is illustrated in Fig. E-6. Since less than 1% of the extracted sources were detected with $mesh = 2$ with no counterpart in the $mesh = 1$ catalogue, while almost 30% of the extracted sources were only detected with $mesh = 1$, the published data (position and photometry) come from the $mesh$ =1 results for the sources which were detected with both values, in order to get a homogeneous set of data. Further quality selection criteria are applied later in the processing (see Sect. 3.2.8), so that only ≈10% of the sources in the published catalogue have been detected with $mesh$ =1 only.

The sources detected only with $mesh = 1$ can be point sources in very crowded regions, where blending effects can occur, so that the most precise analysis is required to properly extract the sources; but they may also be small spots within a background emission pattern rather than true point-like sources. A special MESH flag is included in the catalogue to indicate for which value(s) of $mesh$ a source has been extracted, and the global QUALITY flag is decreased for sources without association between the $mesh = 1$ and the $mesh = 2$ results (see next Section).

3.2.5. Source extraction quality flags

This complex source extraction procedure resulted in a large number of point sources ($\sim 3 \times 10^5$). The quality of the derived photometry as well as the reliability of the extracted sources can be affected by several factors, and different quality flags have been computed to warn the user when effects degrading the photometric quality are present, and to finally estimate the global quality of the point sources.

The MESH flag

As already explained in Sect. 3.2.4, the source extraction procedure combined the results of the extractions performed with $mesh = 1$ and with $mesh = 2$. The MESH flag is set to 1 (resp. 2) for sources which have been detected only with $mesh = 1$ (resp. 2), and to 3 for the sources which could be associated between the two extractions, thus making their reality more trustful.

The NPIX flag

The number of independent measurements of the signal at the position of a source, which takes into account the number of coadded individual exposures, but also the fact

that some exposures might be discarded due to glitches or to the ISOCAM dead column, directly affects the photometric quality. The NPIX flag is the integer part of one tenth of the weighted number of measurements usable at the central position of the source, as given in the third plane of the OLP7 processed FITS files. As each raster position has been observed on average 19×1.5 (see Sect. 2.1) times, typical "good quality" values of this flag are in the range 2 to 4. Note that this flag is rather an indication of the number of good exposures than a number of pixels involved, but we decided to keep the NPIX name, as it appears in the header of the OLP7 processed files.

The EDGE flag

The position of a source with respect to the edges of the raster also affects the derived photometric quality, because the extraction procedure needs a large enough observed area to properly compute the flux density of the source and the background to be subtracted. The EDGE flag is set to 1 when the centre of the source is at a distance between two and five pixels from the edge of the observed raster (taking into account the saw-tooth borders), and to 0 when the distance is greater than five pixels. Sources at less than two pixels from one edge were removed from the catalogue, since their flux density cannot be properly estimated.

The global quality flag Q

By combining the previous quality flags, a global quality estimator was computed according to:

$$q = 10 \times (0.5 - \sigma) - EDGE - M - G + NPIX/10$$

where

- σ is the uncertainty on the flux density as derived by the PSF photometry (Sect. 3.2.3), expressed in magnitude,
- $M = 0$ if the MESH flag is equal to 3, $M = 1$ if MESH is 1 or 2 and the pixel size is 6", and $M = 2$ if MESH is 1 or 2 and the pixel size is 3",
- G = 0 if the distance between the 'inversion' and the 'vision' positions is ≤ 0.5 pixel, G = 1 if this distance is 0.5–1 pixel. Sources with this distance larger than one pixel have been discarded.

Then, according to the distribution of q, the best quality sources have $q \geq 4$ and sources with $q \leq 0$ were not included in the PSC. The remaining range in q has then been divided in three ranges to compute the final quality flag Q, assigning a better quality to well confirmed sources (with MESH = 3), according to:

1. for sources with MESH = 1 or 2:
   - Q = 1 if $0 < q \leq 8/3$
   - Q = 2 if $8/3 < q < 4$
   - Q = 3 if $q \geq 4$
2. for sources with MESH = 3:
   - Q = 2 if $0 < q \leq 8/3$
   - Q = 3 if $8/3 < q < 4$
   - Q = 4 if $q \geq 4$

Finally, a particular treatment was adopted for the 6" pixel observations with the narrow filters LW5, LW6 and LW9. Indeed, the errors in the measured magnitudes for the faintest sources and the completeness factors in these peculiar fields, as derived from artificial source simulations (see Sect. 3.4 and the results in Sect. 3.4.5), are inferior to the "normal" LW2 and LW3 observations. We therefore decided to reduce by one unity the quality flags of the faintest sources, namely those sources with a measured magnitude between the magnitude used to cut the catalogue (Sect. 3.4.6) and 0.5 mag brighter than this (this range was extended down to 1 mag brighter than the limiting magnitude for the very peculiar field FC+01694+00081). When this operation resulted in a quality flag Q = 0, the flag Q was finally set to 1, which already indicates very poor quality.

3.2.6. Distribution of the quality flag Q

The distribution of the final quality flag Q for all the sources in the catalogue is shown for the different filters in Fig. 7. As can be seen, more than one half of the sources have a very good photometric quality (Q = 4). A value of 3 for this flag can also be considered as reasonably good quality. Finally, only $\sim$ 15% of the sources in the catalogue have a moderate photometric quality (Q $\leq$ 2). They should be used with much caution since their reliability is not warranted.

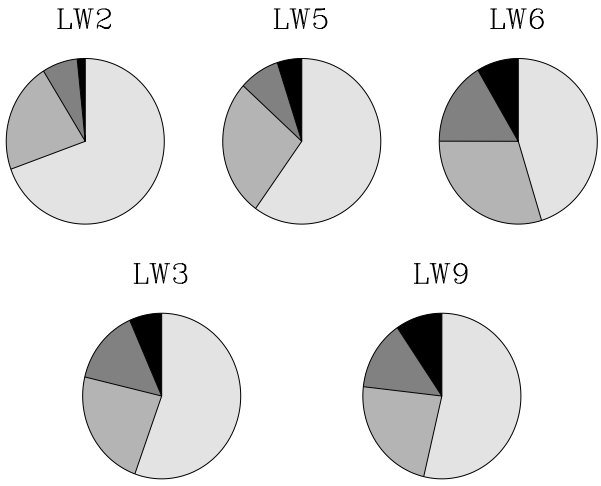

Fig. 7. Distribution of the quality flag Q for the different filters. The gray scale corresponds to the different values of this flag, from 4 (lightest grey) to 1 (darkest grey).

Additional estimates of the reliability of the sources are provided by the analysis of repeated or overlapping

observations (see Sect. 3.5.1), but also by the combination of several wavelengths, including DENIS ones: a source with a moderate quality flag at, for example, 7 μm, but with a good quality association at 15 μm (see Sect. 3.6) finally has a very large probability to be a real source.

3.2.7. Extended sources

The first version of the ISOGAL PSC only contains point sources, and sources of very small extension. The extraction of extended objects will be performed with a dedicated procedure for the second version of the catalogue.

The present version of the PSC contains a small proportion of sources of small extension, with typical sizes around 10-20" (FWHM). These slightly-extended sources are characterised by relatively high values of the photometric uncertainty, with typical $\sigma \approx 0.15$ mag for bright ($F_\nu \approx 1$ Jy) sources, while bright point sources generally have $\sigma < 0.05$ mag. Aperture photometry performed on a small sample of such bright slightly extended sources has shown that their magnitudes can be underestimated by about 1 mag (Schuller 2002). It is planned to perform accurate photometry and to include a relevant extension flag in the second version of the PSC.

3.2.8. Spurious sources

Three kinds of extracted sources are considered as spurious: (1) the "inversion-only" sources, i.e. those found in 'inversion' rasters with no counterpart in the 'vision' rasters (see Sect. 3.2.4), (2) the sources with an inversion-vision association with a large separation ($\geq$0.5 pixel, flag $G = 1$) and with a poor extraction confirmation (flag $MESH < 3$), and (3) the other possible remnants of bright sources. Indeed, the 'vision' method (see Sect. 3.1) does not remove all remnant sources, and remaining remnants of bright ($\geq$ 100 mJy) sources were identified by looking for faint sources within a radius of 0.5 pixel around the exact location of the bright source in the detector at the five successive positions in the raster. They have been removed from the catalogue (see Fig. E-8) and their positions and magnitudes are listed in the catalogue of spurious sources (Sect. 6). Unfortunately, true faint sources which are found at the position of a putative remnant are also considered as spurious, and appear in the catalogue of spurious sources but not in the PSC.

3.3. Photometric calibration

As described in Sect. 3.2.3, the point source flux densities are obtained by applying a PSF fitting procedure to the final mosaic image of the rasters processed in CIA. This method is the best in crowded fields, which is the case for most ISOGAL observed fields. However, our PSF fitting routine only gives relative photometry which still has to be calibrated in an absolute way. This can be done by comparing the photometry resulting from our extraction procedure with that obtained using the same method as for the ISOCAM flux calibration on standard stars (Blommaert 1998; Blommaert et al. 2000). Another important aspect of the ISOCAM flux calibration is the time necessary to reach a stabilised signal after each flux step (Coulais & Abergel 2000). The general flux calibration of ISOCAM was done by observing bright standard stars for long enough times to allow the signal to stabilise (Blommaert 1998). These two aspects of the flux calibration of the ISOGAL catalogue are discussed in the following subsections.

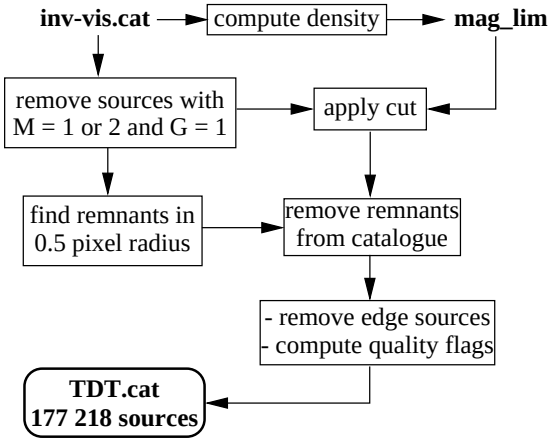

Fig. E-8. Summary of the final steps of the source extraction from individual observations (see Sect. 3.2.5 for the definitions of the M and G flags, and Sect. 3.4.5 for the computation of mag_lim).

3.3.1. Incomplete signal stabilisation

The integration time for the standard ISOGAL observations was $\sim$ 19 frames of 1.12 sec at each raster position. This is too short to allow the signal to stabilise if a change in flux is observed. A correction to this transient problem is applied with the 'inversion' method (see Sect. 3.1). However, this method only allows proper correction for extended emission and not for point sources (Coulais & Abergel 2000). Tests performed on point sources for the ISOCAM calibration show that this method provides a correction in the right direction, but is still insufficient (Blommaert 1998).

A few ISOGAL fields were observed with $\sim$ 56 frames of 1.12 sec per position in order to investigate the effect of the slow detector response. A comparison of a *regular* and a *long* measurement was made by creating two mosaic images (using the standard ISOGAL data reduction techniques with the 'inversion' method). In the first case we simulated a "normal" raster by selecting only the first 19 readouts per raster position in the *long* measurement. In the second case, only the last 30 frames (where one expects to get a better stabilisation) were selected.

The differences in photometry between the two cases, obtained for observations with different configurations, are

given in Table 7. On average, the photometry from the "normal" raster is about 0.2 magnitude too high compared to that from the 30 last frames, which is considered to be close to the stabilised value. An example of the measured differences for the LW2 filter with 6" pixels is shown in Fig. E-9. We preferred making a so-called normal raster from the long raster over simply comparing with a regular raster, observed at the same position, as the latter option increases the scatter in the comparison of the photometry. The same average shift, however, was observed.

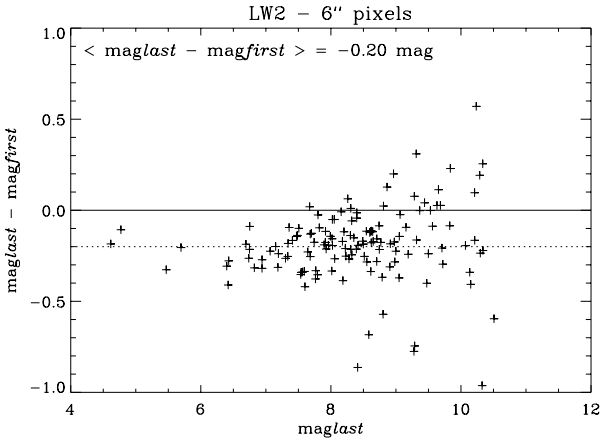

Fig. E-9. Differences in magnitude when considering the first 19 frames (mag_{first}) or the last 30 frames (mag_{last}) for each pointing in a *long* integration time raster, observed with LW2 filter and 6" pixels.

3.3.2. Correction to infinite aperture

The general flux calibration of ISOCAM was established from measurements on standard stars (Blommaert 1998; Blommaert et al. 2000). The observed signal was measured using aperture photometry, which was corrected for the part of the PSF falling outside the aperture. To convert our PSF-fitting photometry to absolute photometry, a comparison was made with photometry obtained using the same techniques as in the ISOCAM general flux calibration. For each filter and pixel size combination, 10 to 30 stars were selected in different fields, and aperture photometry was obtained on the individual ISOCAM images (before they were combined into a raster) within an aperture of radius three and four pixels for 6" and 3" pixel observations, respectively. The sky level was determined from the surrounding pixels. The aperture photometry was corrected for the PSF outside the aperture, as was done in the case of the general CAM calibration. The aperture magnitudes were found to be lower (brighter) than the PSF magnitudes, revealing a bias in the PSF normalisation. The corrections found for the different setups are listed in Table 7.

Table 7. Photometric corrections. This table gives, for each observational setup, the number of isolated stars on which aperture photometry has been performed, the mean value of the difference between aperture and PSF-fitting photometry and the corresponding standard deviation, the mean value of the correction for incomplete signal stabilisation, where the values in parenthesis correspond to *guessed* values when no *long* observation was available for a given setup, and the total needed correction, which is the sum of the two previous ones.

Filter	Pixel	Nb	mag_{ap}-mag_{PSF}	Stabilis.	Total
LW2	3"	11	-0.20 ±0.065	(-0.20)	-0.40
LW2	6"	30	-0.23 ±0.10	-0.20	-0.43
LW3	3"	9	-0.32 ±0.05	(-0.20)	-0.52
LW3	6"	22	-0.28 ±0.10	-0.21	-0.49
LW5	3"	8	-0.17 ±0.08	(-0.20)	-0.37
LW5	6"	10	-0.24 ±0.13	(-0.20)	-0.44
LW6	3"	8	-0.22 ±0.06	-0.20	-0.42
LW6	6"	17	-0.27 ±0.12	-0.20	-0.47
LW9	3"	12	-0.40 ±0.07	-0.14	-0.54
LW9	6"	24	-0.42 ±0.20	-0.17	-0.59

3.3.3. Final correction

As shown in the last column of Table 7, the total correction that has to be applied is between −0.37 and −0.59 mag for the different setups. As the uncertainty on each determined correction is at least 0.1 mag we decided to apply the same constant offset of −0.45 mag to all the sources and for all observational setups. This correction leads to photometry in good agreement with external comparison data, as is explained below.

The first publications based on ISOGAL data made use of a non-corrected photometry. The mid-infrared magnitudes presented there should thus be corrected by a −0.45 mag offset (with a possible ± 0.1 mag additional discrepancy from field to field). This concerns in particular the results published in Pérault et al. (1996), Testi et al. (1997), Omont et al. (1999), Glass et al. (1999), Schultheis et al. (2000) and Felli et al. (2000). Appropriate errata will be published for these papers.

3.3.4. Comparison with template stars

The ultimate check of the calibration must be based on the comparison of the observed with the predicted photometry for stars with known spectra, i.e. standard stars. No established standard star (e.g. from the ISO Ground-Based Preparatory Programme, GBPP, Hammersley et al. 1998) was observed as part of the ISOGAL survey. We therefore searched the Hipparcos Input Catalogue (HIC) for single main-sequence or giant stars which would have well known spectral energy distributions. Three HIC stars were identified which satisfied the above requirement and are sufficiently bright and in a sufficiently clean region of the sky that reliable photometry could be obtained; these stars and their characteristics are listed in Table 8. Appropriate stellar templates for these stars were kindly provided by

Table 8. Template stars: predicted and measured magnitudes. The ISO magnitudes already contain the −0.45 mag correction.

Source designation		Spectral			Predicted mag.		Measured mag.		Predicted - measured	
HIC	HD	type	V	$B-V$	[LW2]	[LW3]	[LW2]	[LW3]	[LW2]	[LW3]
HIC84150	HD155259	A0/A1V	5.66	0.04	5.53	5.64	5.55	5.67	-0.02	-0.03
HIC88142	HD164031	K0III	6.70	1.10	4.20	4.24	4.03	4.04	0.17	0.20
HIC89422	HD167246	K1III	7.11	1.21	4.27	4.27	4.30	4.31	-0.03	-0.04

Dr. M. Cohen. These templates consist basically of the spectrum of either a model atmosphere (for early type star) or of the observed spectrum of a star of similar spectral type (for late-type giants) that was reddened to the known $E(B-V)$ of the target star, and normalised to the known (using published values from the 2nd incremental data release of the 2MASS survey, Skrutskie et al. 1997) near-IR photometry of that star. Finally, these spectra were convolved with the LW2 and LW3 system transmission profiles to derive predicted magnitudes.

The predicted and measured magnitudes are reported in Table 8. The uncertainties in the predicted magnitudes are $\sim \pm 0.15$ mag, and come from (1) the uncertainty in the 2MASS near-IR photometry, (2) a possible mismatch in the spectral type, and (3) uncertainty in the spectral type of the model or of the reference star. The first of these is probably the main contributor to the uncertainty, as in general the extrapolation from the near to the mid-IR is quite straightforward, especially for the early-type stars, which have nearly Rayleigh-Jeans spectra even in the near-IR.

Comparing the predicted and the corrected PSF magnitudes we obtain:

$$mag_{\rm pred} - mag_{\rm PSF} = 0.04 \pm 0.10$$

where the result is the average of all determinations, independent of filter-PFOV combination, and the uncertainty is the variance of the six determinations obtained, though the distribution of these determinations is clearly non-Gaussian.

3.3.5. Cross calibration with MSX

A second check on the photometry is provided by the cross calibration with the published catalogue of bright sources detected by the MSX survey of the Galactic Plane (Price et al. 2001). A comparison with the Band D photometry of MSX, which used a filter similar to the ISOCAM 15 μm filters, showed good agreement between the corrected ISO magnitudes and the MSX ones. For 650 stars (424 observed with LW3 and 226 with LW9) we find:

$$mag_{\rm MSX} - mag_{\rm PSF} = 0.01 \pm 0.40$$

where the uncertainty is the RMS of the measured differences in magnitude. The large width of the distribution is due to the combination of the ISO and MSX photometry uncertainties, and to the intrinsic variability of many of such bright stars. Note that, strictly speaking, this result is valid for the brightest ISOGAL stars that could also be measured by MSX (which means roughly $[15] \lesssim 4.0$). Moreover, the computation of the mean difference in magnitudes was limited to an even brighter sample ($[15] < 3.0$) in order to avoid Malmquist bias. This nevertheless shows that our photometric calibration is reasonably good and in agreement with others.

3.4. Artificial sources

Artificial star experiments (see Bellazzini et al. 2002 and references therein for a general description) were conducted on the ISOGAL images in order to study the effects of a crowded field on the photometric quality and the completeness of the extracted point source catalogue. A procedure was created for adding artificial stars to the ISOGAL images, for extracting the sources with the same pipeline as the one used to generate the ISOGAL catalogue, and for checking how well the input sources are extracted. The procedure that was applied and the main results of this analysis are summarised below.

3.4.1. Description of the procedure

A list of positions of artificial sources was randomly created for a given image dimension, taking care that only one artificial source falls in a fixed spatial box of 20×20 pixels. Interference between artificial stars would, in fact, change the actual crowding and affect the results of the artificial experiment study. Magnitudes were randomly chosen from the observed brightness distribution. A new image was then built by adding the artificial stars and their Poisson photon noise into the original image, using the PSF corresponding to the observational setup. Then, the PSF-fitting extraction procedure was used on the modified image, following almost all the steps we took to extract the sources from the data. The only difference was in the *mesh* parameter of the extraction program (Sect. 3.2.2), which was fixed at 2 for this analysis (to limit the computational time), while we used both $mesh = 1$ and $mesh = 2$ and then correlated the results of the two extractions to produce the Point Source Catalogue. The effects of this parameter on the derived completeness factor are analysed in Sect. 3.4.4. Finally, a cross-correlation was done between the input artificial star catalogue and the output catalogue. Artificial sources having an output magnitude 0.75 mag brighter than their input magnitude were considered lost. In fact, such objects were blended with real sources which were brighter than they were.

Artificial star simulations were conducted on a sample of 6" pixel images (total area ∼2 deg^2) with all available filters, in order to well sample the different crowding levels (the source density ranges from 0.0017 to 0.03 source per pixel), and on all 3" pixel images used for the Point Source Catalogue. For each image, the procedure was repeated between 100 and ∼300 times, depending on the source density and image size. A total of 5×10^3 to 4×10^4 sources were added per raster image in order to achieve statistically significant results.

3.4.2. Effects of crowding

Artificial star experiments enabled us to evaluate both random and systematic photometric errors due to crowding. Mean values and standard deviations of the differences between input and output magnitudes of the recovered artificial stars were calculated per bin of 0.5 input magnitude. The output magnitudes were found brighter than the input ones. This bias is very small for bright stars, but can reach 0.3 magnitude for the faintest ones in the densest fields, where the probability of blending with real stars is higher. Fig. E-10 shows the amplitude of this effect for two extreme cases, for one of the densest and one of the least dense fields.

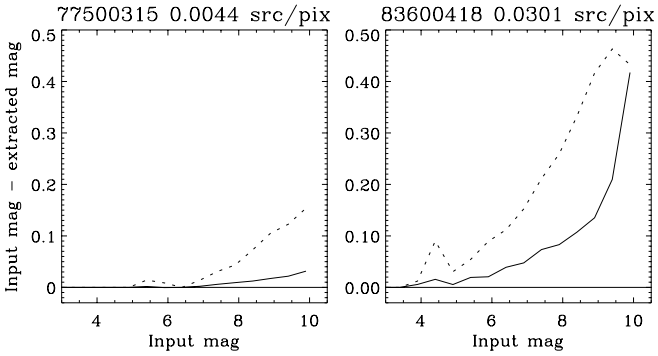

Fig. E-10. Difference between input and extracted magnitudes for two LW2 6" pixel observations. The full lines show the mean values of this difference in 0.5 magnitude bins, and the dotted lines show the standard deviation of the differences in the same bins.

For each observation where artificial sources have been simulated, the magnitude above which the mean value (or the standard deviation) of the difference between input and output magnitudes (the bias) becomes greater than a given value has been computed, and the variations of this magnitude with the source density are reported in Fig. E-11 and Fig. E-12 for the 6" pixel observations. These plots show that the photometric quality remains very good down to the faintest magnitudes in low density regions observed with the broad filters LW2 and LW3, but that we have to limit the catalogues one or two magnitudes brighter than the faintest extracted sources in order to ensure low systematic errors and accurate measurements in the densest fields, and in the few peculiar fields which needed observations with narrow filters. Similar results for the 3" pixel observations are reported in Table 9.

Table 9. Results of the artificial source simulations on all 3" pixel observations used in the PSC: ISO observation number, filter, density expressed in source/pixel, and magnitudes above which the mean value of the bias reaches 0.1 mag (mag_1), the corresponding standard deviation reaches 0.3 mag (mag_2), and the completeness factor is below 50% (mag_3).

ION	Filter	Density	mag_1	mag_2	mag_3
78900220	LW2	0.0092	>10.00	>10.00	>10.00
84001222	LW2	0.0058	>9.70	>9.70	>9.70
84001724	LW2	0.0089	>9.90	>9.90	>9.90
31300135	LW5	0.0187	7.97	7.41	8.04
31300236	LW5	0.0173	8.16	7.60	8.25
31300433	LW5	0.0140	8.51	7.67	8.44
31300734	LW5	0.0165	7.95	7.31	8.00
78900221	LW3	0.0034	>8.20	>8.20	>8.20
84001223	LW3	0.0023	>8.20	>8.20	>8.20
84001725	LW3	0.0034	>8.20	>8.20	>8.20
82700140	LW9	0.0118	6.90	6.06	6.79
82800341	LW9	0.0100	6.77	5.84	6.58
83600308	LW9	0.0107	7.22	6.40	7.02
83800712	LW9	0.0089	7.67	7.18	7.48
84100259	LW9	0.0095	7.59	6.96	7.33

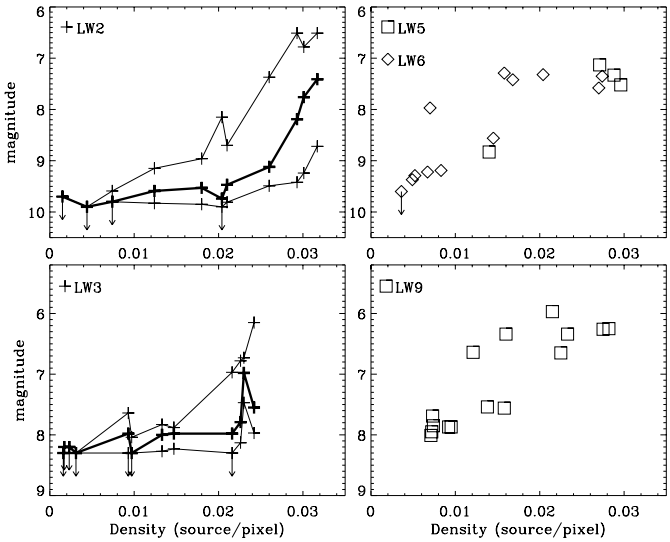

Fig. E-11. *Left*: broad filters. Magnitudes above which the **mean value of the errors** of the extracted magnitudes becomes greater than 0.05 mag (top line), 0.1 mag (middle thick line) or 0.2 mag (bottom line), as a function of source density, for the 6" pixel observations. The vertical arrows are lower limits.*Right*: narrow filters. Only the magnitudes where the mean value of the bias reaches 0.1 mag are reported. The different symbols correspond to the different filters, as indicated in the upper left corner of each panel.

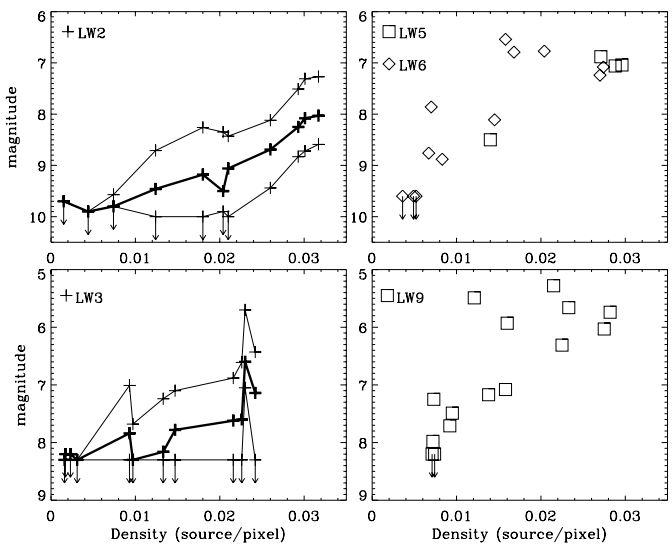

Fig. E-12. *Left*: broad filters. Magnitudes above which the **standard deviation of the errors** in the extracted magnitudes becomes greater than 0.2 mag (top line), 0.3 mag (middle thick line) or 0.4 mag (bottom line), as a function of source density, for the 6" pixel observations. *Right*: narrow filters. Only the magnitudes where the standard deviation of the bias reaches 0.3 mag are reported. The symbols are the same as in Fig. E-11.

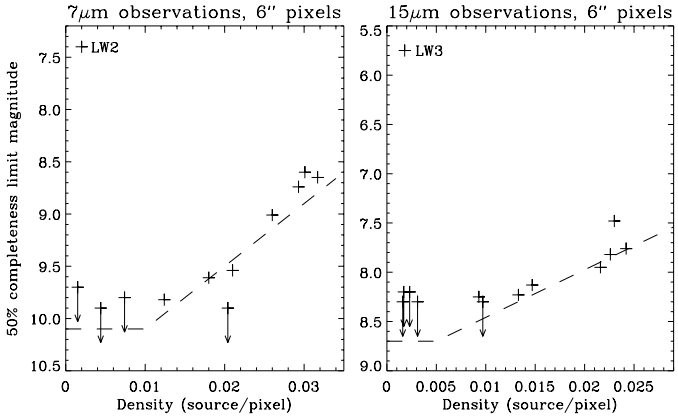

Fig. E-13. a) Completeness limit for artificial sources as a function of source density for 7 μm, 6" observations with the broad LW2 filter. For each observation, the magnitude above which the fraction of recovered sources is below 50% is reported. The dashed line shows the limiting criteria adopted from these results (see Sect. 3.4.5 and Eq. (2)). b) same as a) for 15 μm, 6" observations with the broad LW3 filter. The dashed line shows the limiting criteria that we applied to LW3, 6" observations (Eq. (3)).

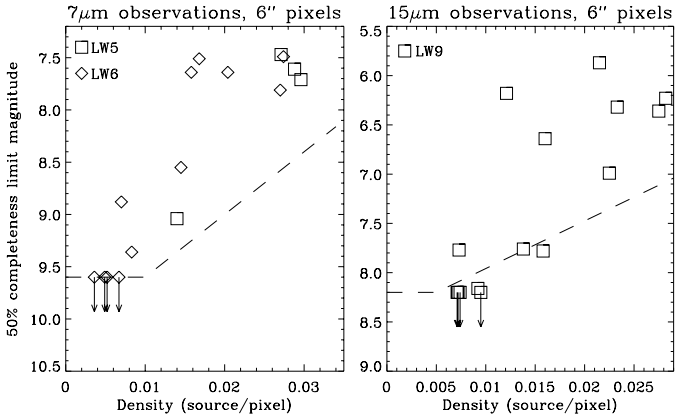

Fig. E-14. Same as Fig. E-13 for the 6" observations with narrow filters. The symbols are the same as in Fig. E-11. The dashed lines show the limiting criteria adopted from these results for LW5 and LW6 6" observations (Eq. (4), left panel) and for LW9, 6" observations (Eq. (5), right panel).

3.4.3. Completeness

Another result of the artificial star analysis is the quantification of the completeness of the extraction. Indeed, for each observation, we can plot the fraction of simulated sources which were retrieved as a function of input magnitude. We observe a smooth curve which drops for the faintest magnitudes. The magnitude where this fraction becomes less than 50% depends on the density of the field, and is summarised in Fig. E-13 and Fig. E-14 for the 6" pixel observations with broad and narrow filters, respectively, and in the last column of Table 9 for the 3" pixel observations. Again, these results show that the catalogues are at least 50% complete down to the faintest end in the least dense fields, but that more care has to be taken in dense regions in order to achieve a good completeness level.

3.4.4. Effects of the *mesh* parameter

For a few ISOGAL observations, we also run the artificial sources procedure with the *mesh* extraction parameter set to 1. The results we derived are summarised in Table 10.

As can be seen, the effects of this parameter are relatively small (up to 0.1 magnitude difference between $mesh = 1$ and $mesh = 2$) for 7 μm observations, and for 15 μm observations with 3" pixels. But the magnitude where the completeness factor is below 50% can be underestimated by more than 0.3 magnitude for the 15 μm observations with 6" pixels. These effects have been taken into account to derive the magnitudes at which the published catalogues have been limited, in order to ensure a good level of reliability (see next section).

The effect of reducing the *mesh* parameter on the completeness of the 15 μm 6" observations can be interpreted as a more efficient way for extracting blended sources with $mesh = 1$. Indeed, the angular resolution of the ISO telescope at $\lambda = 15\,\mu$m is ≈ 6", which is the size of one pixel. Therefore, analysis with the thinnest mesh is required for properly extracting blended or very close sources; however, the reality of the sources extracted with $mesh = 1$ only is not obvious, as discussed in Sect. 3.5.3.

Table 10. Effects of the *mesh* parameter on the derived 50%-completeness magnitude.

TDT	Filter	Pixel	mag (50%compl.)	
			mesh=2	mesh=1
31300135	LW5	3"	8.04	8.12
83600417	LW2	3"	9.61	9.67
84100428	LW2	6"	9.01	9.22
84100926	LW2	6"	8.65	8.70
82700140	LW9	3"	6.79	6.88
83600522	LW3	3"	>8.30	>8.30
48002270	LW3	6"	8.13	>8.30
84100927	LW3	6"	7.76	8.08
32500238	LW3	6"	7.95	>8.30
31300901	LW9	6"	6.36	6.72

3.4.5. Final results: limiting magnitudes

We finally chose to use the 50% completeness criterion to define the limiting magnitudes, and the results are generally consistent with the magnitudes above which the bias reaches 0.1 magnitude and its standard deviation reaches 0.3 magnitude. We derived relations between source density and limiting magnitudes for the different observational setups. We make a distinction between the core of the ISOGAL survey observed with broad filters and 6" pixels and the peculiar observations of difficult fields observed with narrow filters and 6" or 3" pixels.

A) 6" pixel observations with broad filters

For the 6" pixel observations with LW2 and LW3 filters, we computed linear relations from the results plotted in Fig. E-13, as indicated by the dashed lines. Note that some points are above (toward brighter magnitudes) these lines, but that this is consistent with the effect of the "mesh" parameter, since the results we obtained with $mesh = 1$ are near or below these lines. The linear relations are:

– for LW2 observations:

$$mag_{\rm lim} = \begin{cases} 10.1 & \text{if } d \leq 0.01, \\ 10.7 - 60. \times d & \text{if } d \geq 0.01, \end{cases} \quad (2)$$

where d is the source density expressed in source/pixel. Thus, the limiting magnitude ranges from 10.1 to 8.8, corresponding to limiting flux densities between 8 and 27 mJy.

– for LW3 observations:

$$mag_{\rm lim} = \begin{cases} 8.7 & \text{if } d \leq 0.005, \\ 8.9 - 40. \times d & \text{if } d \geq 0.005, \end{cases} \quad (3)$$

Here, the limiting magnitude ranges from 8.7 to 7.7, and the associated flux density ranges from 6.5 to 16 mJy.

When we apply these relations to the catalogues extracted from the observations for which we have run the artificial sources procedure, we obtain biases (Sect. 3.4.2) in a 0.5 magnitude wide bin centred on $\rm mag_{lim}$ around 0.1 mag and associated standard deviations generally around 0.3 mag (see Fig. E-15).

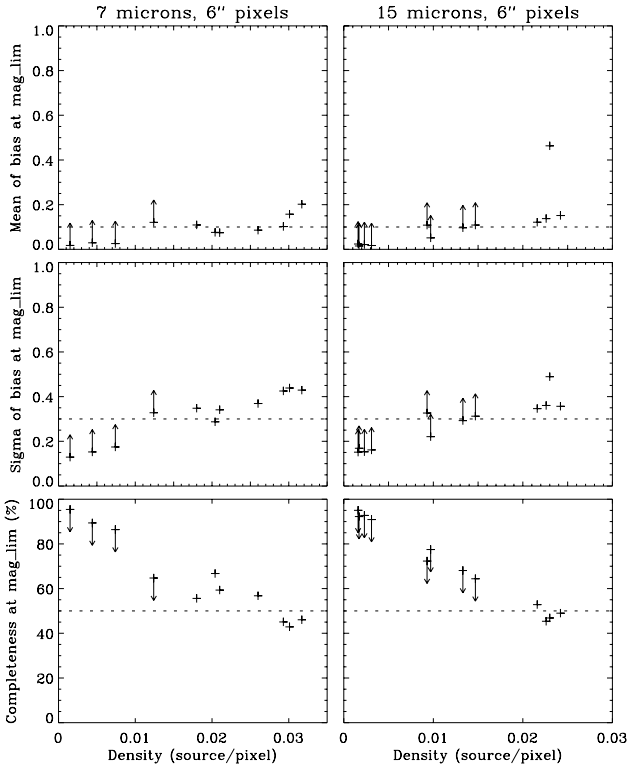

Fig. E-15. Mean of bias (top panel), σ of bias (middle panel) and completeness factor (bottom panel) in a 0.5 magnitude wide bin centred at $\rm mag_{lim}$, for LW2 and LW3 observations with 6" pixels. The vertical arrows are lower or upper limits, and correspond to cases where $\rm mag_{lim}$+0.25 is greater than the maximum magnitude of simulated sources.

B) 6" pixel observations with narrow filters

The results of our artificial source simulations show that the completeness level is generally worse in LW5, LW6 and LW9 observations, which can be interpreted as an effect of the much brighter diffuse background in the peculiar regions which needed the use of such narrow filters. Therefore, we applied 0.5 magnitude brighter cutting criteria for the 6" observations with these filters:

– for LW5 and LW6 observations:

$$mag_{\rm lim} = \begin{cases} 9.6 & \text{if } d \leq 0.01, \\ 10.2 - 60. \times d & \text{if } d \geq 0.01, \end{cases} \quad (4)$$

– for LW9 observations:

$$mag_{\rm lim} = \begin{cases} 8.2 & \text{if } d \leq 0.005, \\ 8.4 - 40. \times d & \text{if } d \geq 0.005, \end{cases} \quad (5)$$

The problems are indeed much more severe in these peculiar fields, and the standard deviation exceeds 0.5 mag

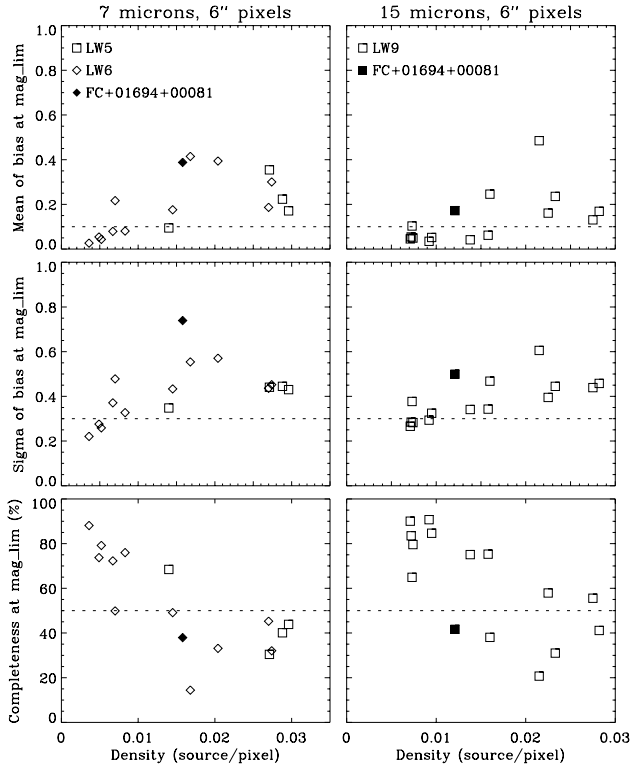

Fig. E-16. Same as Fig. E-15 for 6" observations with the narrow filters LW5, LW6 and LW9. A 0.5 magnitude wide bin was centred at mag_{lim}-0.5 (or mag_{lim}-1 for the peculiar FC+01694+00081 field, plain symbols) to compute the results.

in a few cases. Therefore we decided to decrease the quality flags (see Sect. 3.2.5) for the sources with magnitudes between mag_{lim}-0.5 and mag_{lim}, but the derived bias in a bin centred at mag_{lim}-0.5 remains rather high in a few very peculiar fields (Fig. E-16). In particular, we extended the range in which we decreased the quality flags down to mag_{lim}-1 for the most difficult FC+01694+00081 field located in the M16 nebula.

C) 3" pixel observations

The situation is slightly more complicated for the 3" pixel observations, because they are too few and peculiar to allow a global statistical treatment. They can be sorted in two distinct categories: (i) observations with narrow filters near the Galactic Centre, and (ii) observations with broad filters in low source density regions. Artificial source simulations have been run on all the 3" pixel observations used in the PSC (see Table 9), and the results show good agreement between the different observations with a given filter. Therefore we used a single limiting magnitude for each filter, and the different values are given in Table 11.

These limits give reasonably good results in terms of bias and completeness, as illustrated in Fig. E-17.

Table 11. Limiting magnitudes used to cut the catalogues for 3" pixel observations.

Filter	LW2	LW5	LW3	LW9
mag_{lim}	10.0	8.4	8.5	7.0

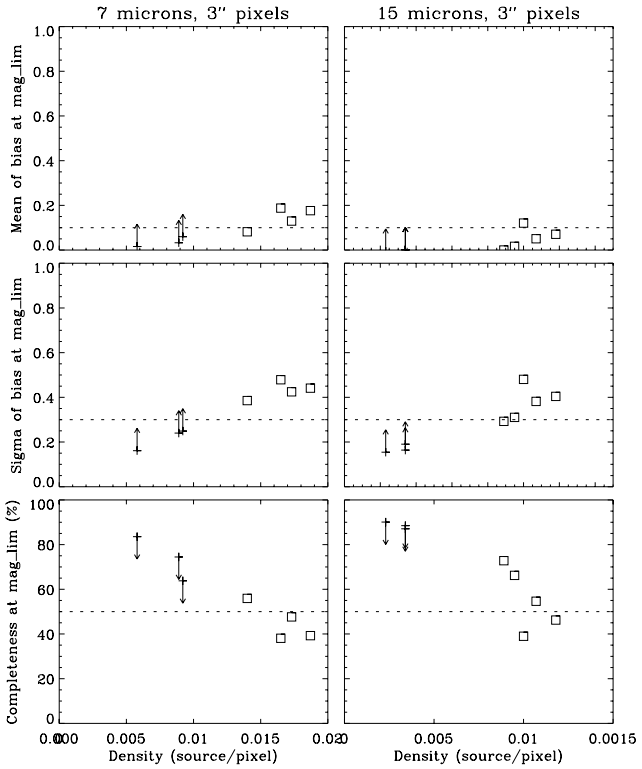

Fig. E-17. Same as Fig. E-15 for all 3" pixel observations, using the mag_{lim} quoted in Table 11 for all filters. The symbols are the same as in Fig. E-11.

3.4.6. Conclusion: limiting the Point Source Catalogue

The distribution of the limiting magnitudes, as defined in the previous section (Eqs. (2), (3), (4) and (5) for 6" pixel observations, Table 11 for 3" pixel observations) for all ISOGAL observations is shown in Fig. 18. Since most observations were done with the broad LW2 and LW3 filters, these histograms show that the typical reached sensitivity is around 20 mJy at 7 μm and 12 mJy at 15 μm.

When we apply these relations to all the ISOGAL catalogues, we eliminate ≈25% of the sources. This photometric cut is far more severe for moderate quality sources than for good quality ones: if we consider the QUALITY flag as defined in Sect. 3.2.5, it appears that about one half of the sources with QUALITY = 1 or 2 are discarded, while ∼ 30% of the sources with QUALITY = 3 and ∼ 12% of the sources with QUALITY = 4 are removed by this cut.

A histogram of the fraction of discarded sources is plotted in Fig. E-19 and shows that in most fields (≈80%) we discard less than 35% of the sources. Only three observations have a resulting fraction of lost sources above 50%. These are LW9, 3" observations close to the Galactic

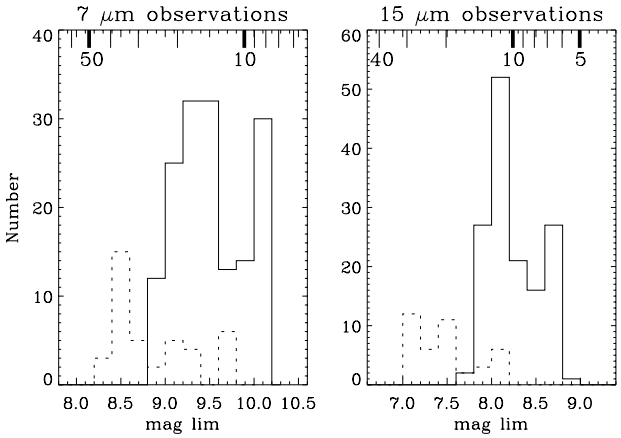

Fig. 18. Distribution of the magnitudes mag_{lim} at which the catalogues have been cut for the broad filters LW2 and LW3 (full lines), and for the narrow filters (dotted lines). However, note that, for the narrow filters, the data with magnitudes higher than mag_{lim}-0.5 are of poor quality (see text, Sect. 3.4.5 B). The logarithmic scales at the top of each panel show the corresponding flux densities in mJy for LW2 and LW3. A small correction has to be applied for the corresponding flux densities with narrow filters (see Table 1).

Centre, where the confusion is the most severe, so that such a strong limiting criterion (mag_{lim} = 7.0, Table 11, corresponding to 28 mJy in flux density) is really needed to limit the number of spurious sources.

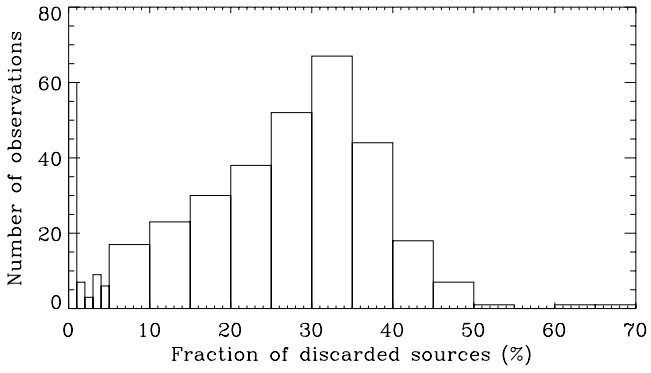

Fig. E-19. Histogram of the fraction of discarded sources for all ISOGAL observations used for the PSC.

3.5. Repeated observations

3.5.1. Overlapping 6" observations

A few ISOGAL fields have been observed twice or more with exactly the same observational setup (filter and pixel size), and a large number of fields have overlapping regions. The total surface of such repeatedly observed areas is ~ 0.7 deg^2. Table 12 shows the observed area and the main results for each observational setup.

Table 12. Main results of the comparison of repeated observations

Filter	Overlap surface (deg^2)	Nb. of sources	$\langle\Delta mag\rangle$	RMS
LW2	0.166	2793	0.008	0.21
LW6	0.098	1974	0.005	0.22
LW3	0.275	2244	0.009	0.23
LW9	0.111	1250	0.007	0.28
Total	0.650	8261	0.003	0.23

A complete analysis of these repeated observations was performed as follows. First, an offset correction was applied to one catalogue so that the coordinates of the sources match those in the other. Then, the true area of overlap was determined by checking the boundaries of each raster image and removing 12 pixels from the external edges, to avoid the saw-tooth zones in which sources can be lost because of edge effects. Then, each source of one observation has been looked for in the other one, within a search radius equal to one pixel, and the resulting products are: 1) the fraction of sources which are recovered in both observations per bin of magnitude, and 2) the difference in magnitude between the two observations. Note that in about two thirds of the cases, a large delay (more than 100 days) exists between the two observations, so that the variability of some sources can increase the observed errors (this is particularly true for bright sources). Therefore the quoted standard deviations in Table 12 are slightly above the true photometric uncertainty of the final catalogue multiplied by $\sqrt{2}$.

Fig. E-20 summarises the results for all overlapping observations in the different filters. A few points clearly deviate from the mean distribution, with errors up to 3 magnitudes, and this can be explained by the variability of some sources, especially for strong sources, but also by wrong associations during the overlap analysis.

3.5.2. Rough completeness estimate

The histograms in the lower part of Fig. E-20 clearly show that the catalogues are not at least 50% complete down to the faintest magnitudes, since more than one half of the sources in the faintest bins are not associated between the two observations. It is however difficult to accurately estimate the completeness by this method, as neither of the two catalogues is complete. It is nevertheless possible to have a rough estimate by comparing the catalogue extracted from a 6" pixel observation with the more complete one, extracted from a 3" pixel observation of the same region. Then we can compute the magnitude above which the fraction of 3" sources found in the 6" catalogue is below 50%.

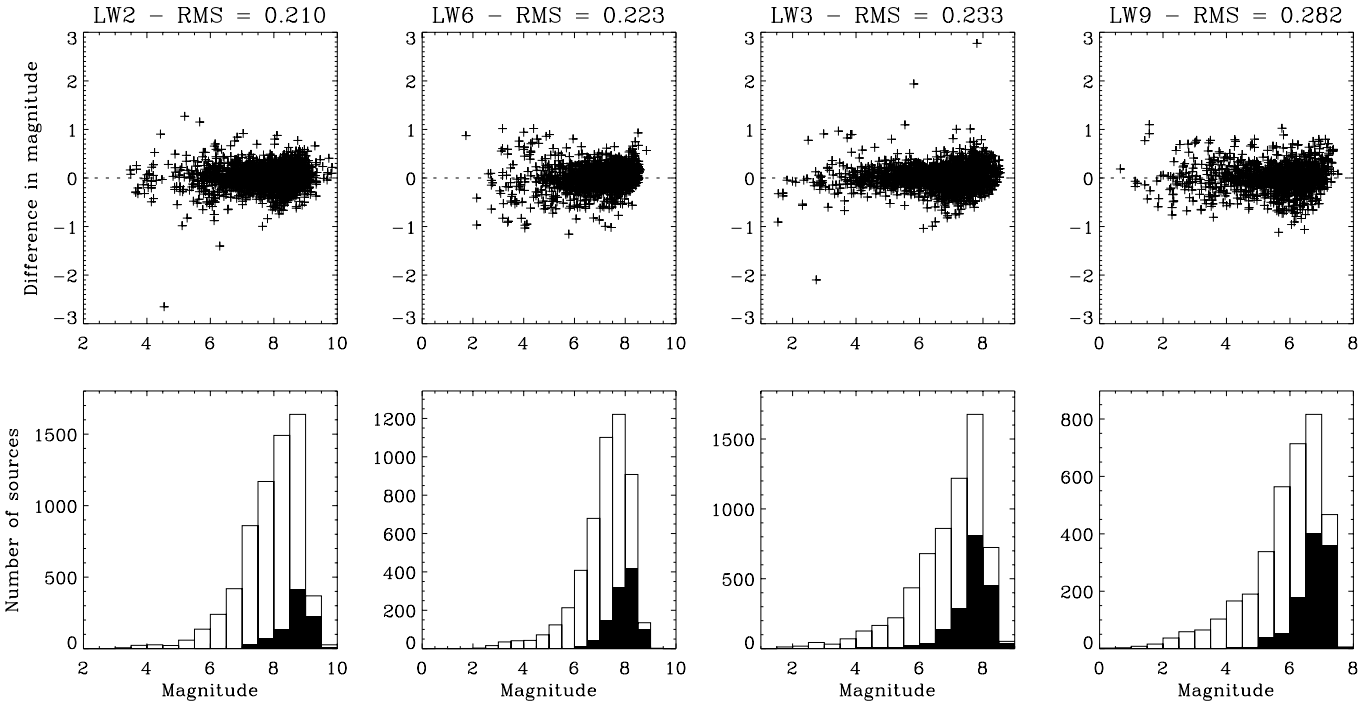

Fig. E-20. Results of the comparison between overlapping 6" pixel observations for the LW2, LW6, LW3 and LW9 filters. The upper panel shows the difference in the magnitudes extracted from both images versus the magnitudes measured in one image. The lower panel shows the total distribution of magnitudes from both observations (clear histogram), and the distribution of magnitudes for the sources of both catalogues which could not be associated between the two observations (plain histogram).

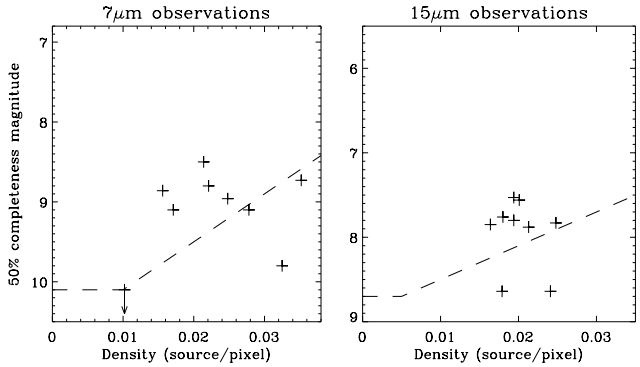

Fig. E-21. a) Results of the comparison between 3" and 6" overlapping LW2 observations. The magnitude above which less than 50% of the 3" sources are found in the 6" catalogue is plotted against the 6" source density in the overlapping region. The dashed line shows the cutting criteria we adopted from the results of the artificial source simulations. b) same for 15 μm observations. The dashed line shows the cutting criteria for LW3 filter.

A) Broad filters

The results for the LW2 and LW3 broad filters are plotted in Fig. E-21. The (approximative) 50% completeness magnitudes we can derive by these comparisons is more or less consistent with the results we derived from the artificial source analysis (Sect. 3.4.5), and thus also with the cutting criteria, within a range of about 0.5 magnitude in most cases. We find however magnitudes slightly brighter than from the artificial source analysis; this may be partly explained by a larger number of spurious sources in the catalogue extracted from the 3" observations, thus a number of faint 3" sources are not found in the 6" observations because they are spurious rather than because of completeness limit. Moreover, the area where the 3" and the 6" observations overlap is very small in most cases ($\lesssim 0.01$ deg^2), and there is a large uncertainty on the results because of the small number of sources.

Finally, most of the areas where two observations overlap are located near the edge of at least one raster, where the NPIX number (Sect. 3.2.5) is generally lower. Thus the quality (photometric accuracy and completeness level) of the sample of sources used for this analysis is not typical of the regular PSC. In addition, the fields used for this analysis are among the most difficult ones, located in the close vicinity of the Galactic Centre or in the molecular ring. Only two fields are located outside the Galactic disk, and the source extraction is much less affected by the background in these cases; these correspond to the points well below the dashed lines in Fig. E-21.

B) Narrow filters

For the observations with narrow filters, the 50% completeness magnitudes are also consistent within 0.5 mag

with the results of the artificial source analysis in some cases, but there are also a few cases where they are well above (typically one magnitude brighter) the limiting magnitudes at which we cut the catalogues (Fig. E-22). All these observations are located very close to the Galactic Centre, where the effects of confusion and the bright diffuse background clearly decrease the completeness level of the observations. This is in fact consistent with the results of the artificial source simulations, which showed that the bias and uncertainty of the photometry are relatively high and the completeness becomes relatively low at least 0.5 mag brighter than the cutting limit. Therefore we decreased the quality flag of the sources in this magnitude range (see Sect. 3.4.5 B)).

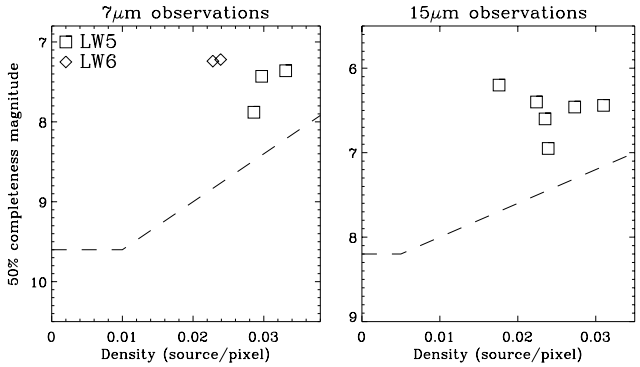

Fig. E-22. Same as Fig. E-21 for the narrow filters LW5 and LW6 (left panel), and LW9 (right panel).

3.5.3. Reality of the extracted sources

An additional check of the reality of the sources can be performed as follows. The sources extracted from 6" pixel observations should also be found in a 3" pixel observation of the same region, because the sensitivity is generally greater in the latter, since the source extraction is much less limited by confusion. Also sources detected at one wavelength and with a good quality association at another ISO or DENIS wavelength have a very large probability to be real. But sources found only in a 6" pixel observation, with counterparts neither in the overlapping 3" pixel observation nor at other wavelengths (or with a bad quality association) may be spurious.

From the same set of overlapping 3" and 6" observations as that used in the previous section, we have determined that the overall fraction of such doubtful sources is very small (∼7%), with a large difference between the 7 μm (∼4%) and the 15 μm (∼11%) sources. This fraction also strongly depends on the quality of the sources, and ranges from less than 1% (at both wavelengths) for sources with quality flags Q = 4, to ∼15% (resp. ∼30%) for sources with Q = 1 or 2 or with MESH = 1 or 2 at 7 μm (resp. at 15 μm). Therefore sources with quality flags less than 3 should be considered with extreme caution, especially at 15 μm.

3.6. 7-15 μm cross-identification

3.6.1. Astrometric correction

The initial astrometric accuracy of the ISOCAM data is limited by the errors in the pointing of the telescope and in the positioning of the lens wheels. According to Table 4.6 in Blommaert et al. (2001), the uncertainty in the satellite pointing amounted to 3", while the lens wheel jitter resulted in an additional uncertainty of up to two pixels in the direction of the movement of the lens. The global astrometric uncertainty can thus reach ∼ 10" (see also Ott 2002), and the offset between two independent observations can reach twice this value. Therefore an offset correction between the 7 μm and the 15 μm observations was needed before the two catalogues could be cross identified. This offset was determined by pairing all the sources of one catalogue with all the sources of the other one, then computing the distributions of offsets in both galactic longitude and latitude, and finally taking the modal values as the global offsets between the two observations. The resulting distances are typically of order a few arcseconds, but can reach 15" as shown in Fig. E-23, in agreement with expectations.

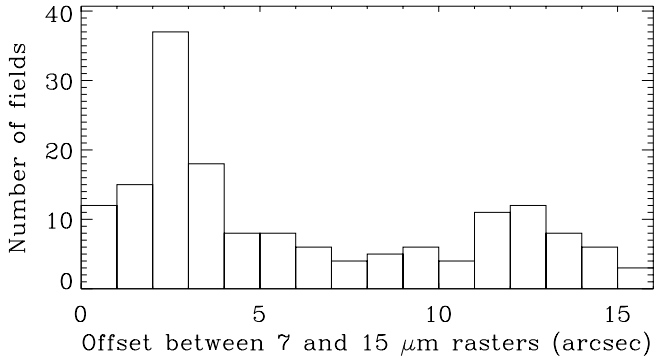

Fig. E-23. Distribution of offset distances between 7 μm and 15 μm observations before astrometric corrections for all ISOGAL FC fields.

In addition, there can be a small error in the positioning of the individual images within the final raster, due to a combination of possible long term drifts and the lens wheel jitter. Only very small amplitude "distortion" effects have been observed, but a low order polynomial correction was systematically applied to the 15 μm coordinates to best match the 7 μm ones. The coefficients of this distortion correction were computed from the residual offsets between the two sets of coordinates, when cross associating the two catalogues after the global (translation) offset correction.

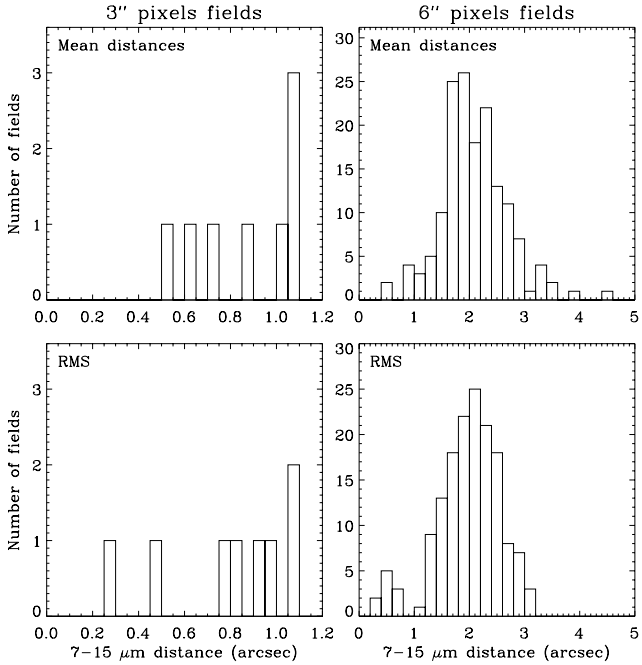

Fig. 24. Top panel: distribution of the mean values of the separations between associated 7 μm and 15 μm sources after astrometric correction in all ISOGAL FC fields. Bottom panel: distribution of the standard deviations of these separations.

3.6.2. Source associations

After the 15 μm coordinates were corrected to match those at 7 μm, an association between 7 μm and 15 μm sources was performed with a search radius equal to two pixels. This rather large radius was chosen in order not to miss 7–15 μm associations for slightly extended sources, and because the density of 15 μm sources is low enough to limit the probability of chance associations to a few percent in most cases. Indeed, the chance probability of finding a 15 μm source within the search radius $R_{\rm s}$ can be computed according to:

$$P = density(15\ \mu\mathrm{m\,sources}) \times \pi \times R_{\rm s}^2 \qquad (6)$$

However, this expression severely overestimates the final fraction of false (chance) associations, since true associations exist with association distances generally much smaller than $R_{\rm s}$, and only associations with the smallest separation are retained. The value of P ranges from 2.5% to 10% for the central fields with 3" pixels, from 0.5% to 10% for the high longitude ($|l| \gtrsim 30°$) fields with 6" pixels, and from 7 to 25% for the most numerous fields in the inner Galactic disk with 6" pixels.

Finally, no special problem was encountered for these associations, and the mean values of the 7–15 μm separations are typically in the range 1–3" in all ISOGAL FC fields, with standard deviations in the same range, as shown in Fig. 24. At the end of this step, the catalogued source coordinates are the most accurate available, namely the 7 μm coordinates for the sources detected at 7 μm, or the 15 μm coordinates translated to the 7 μm referential for the 15 μm sources with no 7 μm association in the FC fields. We kept the initial 15 μm coordinates only for the sources in FB fields without 7 μm observations. Nevertheless, no correction has been applied at this stage in FB fields for the lens wheel jitter, so that these coordinates may be affected by a constant offset of up to ∼10".

3.6.3. The 7–15 μm association quality flag

Finally, a 7–15 μm association quality flag is computed for each associated source. The value of this flag is defined as follows:

4 : the separation between the 7 μm and the 15 μm sources is ≤ 1 pixel and there is only one possible association within a radius of 2 pixels;
3 : the separation is still ≤ 1 pixel but there is another 15 μm source at less than 2 pixels;
2 : the separation is between 1 and 2 pixels, and there is no other source within a radius of 2 pixels;
1 : the separation is between 1 and 2 pixels, and there are at least 2 sources within a radius of 2 pixels.

The distribution of the values of this flag is shown in Fig. 25. A very large majority of the associated sources have a very good quality of association: 87% of the associations have Q_{7-15}=4 and 6.4% have Q_{7-15}=3. Only ∼ 6% of these flags are equal to 2 and fewer than 0.3% are equal to 1, corresponding to an association distance larger than one pixel.

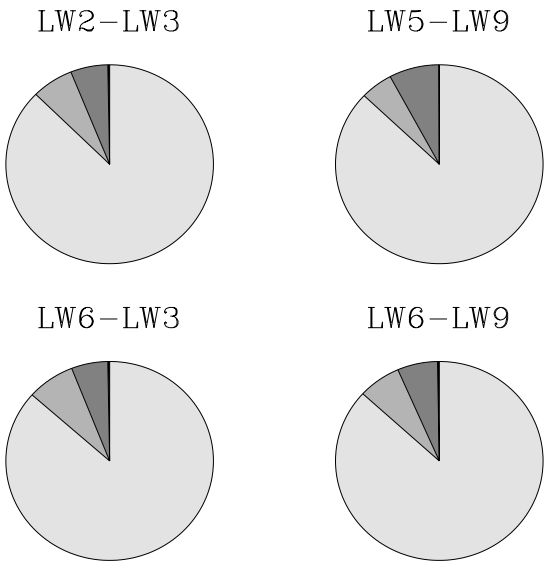

Fig. 25. Distribution of the values of the 7–15 μm association quality flag for the different combinations of 7 and 15 μm filters. The gray scale corresponds to the different values of this flag, from 4 (lightest gray) to 1 (darkest gray). Only very few sources have this flag equal to 1, so that the darkest gray is hardly visible in these plots.

Table 13. Format of DENIS observations (12' × 12' images) Table (version 1)

Col.	Name	Format	Units [range]	Description
1	Name	a7		image number
2	date	a6	YYMMDD	date of observation
3	j_day	i4		Julian day of observation - 2450000
4	RA	f8.4	deg	RA (J2000) of image centre
5	Dec	f8.4	deg	Dec (J2000) of image centre
6	G_lon	f7.3	deg [-180–+180]	Galactic longitude of image centre
7	G_lat	f7.3	deg [-90–+90]	Galactic latitude of image centre
8	q_I	i1		quality flag of I image
9	q_J	i1		quality flag of J image
10	q_K	i1		quality flag of K_s image

However, 19% of the sources detected at 15 μm within the area also observed at 7 μm have no association, while 47% of the 7 μm sources in the common area have no 15 μm counterpart. This large difference is explained by the deeper sensitivity of the 7 μm observations, as compared to the 15 μm ones.

4. DENIS observations of the central Galaxy

In addition to these mid-infrared wavelengths, all the observations in the southern hemisphere (almost 95% of the total area) have been systematically cross-identified with the DENIS (Epchtein et al. 1994, 1997) data, which provide measurements in the three near infrared bands I, J and K_s.

4.1. The DENIS "Bulge" project

In coordination with the ISOGAL project, dedicated observations with the DENIS instrument on the ESO 1 meter telescope at La Silla have been performed, along the inner Galactic plane, between -30 and +10 degrees in galactic longitude, -2 and +2 degrees in latitude, (± 4 degrees in the inner Bulge) using a specific technique (Simon et al. in preparation). The individual images (12'x12') were taken in a raster mode, covering typically 3 square degrees (see Fig. E-26). Between +10 and +30 degrees in longitude, regular 30° DENIS strips (see Epchtein et al. 1994) were used, with a special reduction procedure.

All the DENIS images which have been used to build the ISOGAL PSC are described in the Table of DENIS Observations, whose format is given in Table 13, and a galactic map of the DENIS "Bulge" project observations is shown in Fig. E-26.

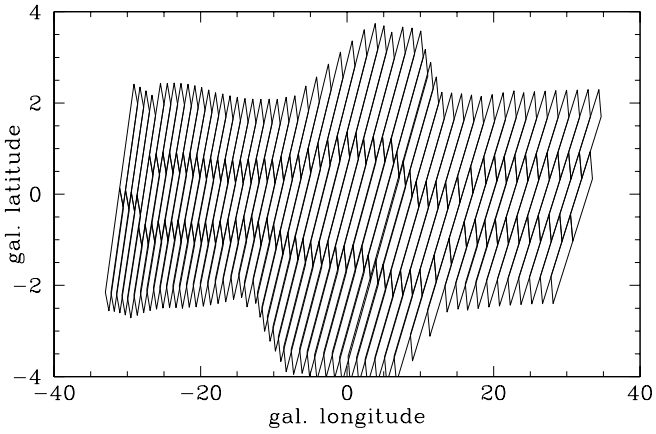

Fig. E-26. Galactic map of the observations for the DENIS "Bulge" project.

4.2. Data processing and accuracy

The source extraction has been made through PSF fitting, using the same extraction code as for ISOCAM images. The PSF is modelled in 9 squares on each 12'×12' individual image and adjusted with respect to the source position. The derived correlation factor gives an evaluation of the photometric uncertainty of the source extraction. For each band, we preserve only the sources with a correlation factor greater than 0.6. The correlation factors are given for each DENIS source in the ISOGAL PSC (Sect. 5).

The saturation of DENIS detectors occurs around magnitude 10 in I, 7.5 in J and 6 in K_s, and results in severely underestimated flux densities. Therefore, the brightest DENIS sources have been removed from the catalogue.

The absolute photometry results from the zero point derived from standard stars observed through the night. A mean value is applied. These magnitudes can be converted to flux densities using the zero points given in Table 14 (from Fouqué et al. 2000).

The limiting sensitivity is about 0.05 mJy (mag. 19) in I, 0.5 mJy (mag. 16) in J and 2.5 mJy (mag. 13.5) in K_s but the extraction can become confusion limited in the dense Galactic environment. The relative accuracy of the photometry is checked through the comparison of the measurements in the overlaps (2' between adjacent images). The present accuracy for the whole set of observations is illustrated in Fig. E-27 and Fig. E-28. The average

Table 14. Isophotal wavelengths and zero point flux densities for the three DENIS bands

Band	$\lambda_{\rm iso}$ (μm)	F_ν (Jy)
I	0.791	2499
J	1.228	1595
$K_{\rm s}$	2.145	665

differences are better than 0.03 mag down to magnitudes 17 in I (standard deviation <0.1 mag), 14 in J and 12 in $K_{\rm s}$ (standard deviation <0.2 mag), which remains very good given the difficulty inherent to such dense regions.

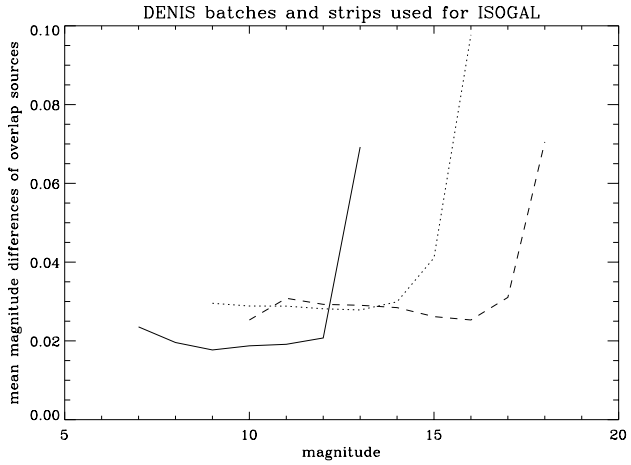

Fig. E-27. DENIS mean absolute magnitude differences in image overlaps for the whole set of Bulge observations for I (dashed line), J (dotted line) and $K_{\rm s}$ (solid line).

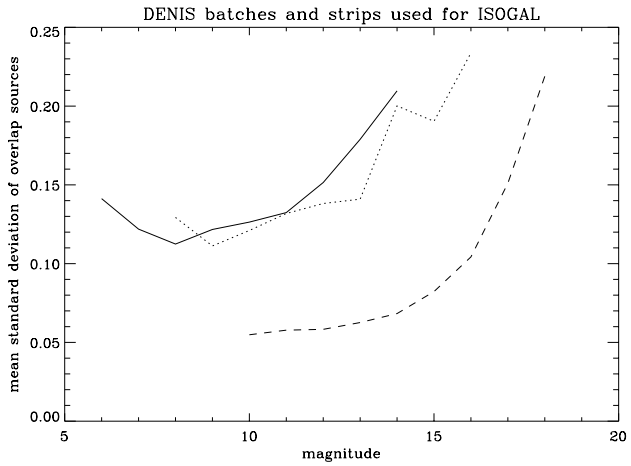

Fig. E-28. DENIS mean standard deviation of magnitude differences in image overlaps for the whole set of Bulge observations for I (dashed line), J (dotted line) and $K_{\rm s}$ (solid line).

Finally, an image quality flag has been evaluated from the overlapping regions of each DENIS frame covering the ISOGAL rasters. In each band the standard deviation of magnitude differences over a defined magnitude range is calculated (see Table 15) and we assigned a quality flag ranging from 0 (very bad) to 3 (very good). Fig. E-29 shows the distribution of the quality flags in each filter.

Table 15. Definition of the DENIS image quality flags

	mag. range	sigma range			
Flag		0	1	2	3
I	11-16	> 0.15	0.1 -0.15	0.07-0.1	< 0.07
J	9-14	> 0.20	0.16-0.20	0.13-0.16	< 0.13
$K_{\rm s}$	7-12	> 0.20	0.16-0.20	0.13-0.16	< 0.13

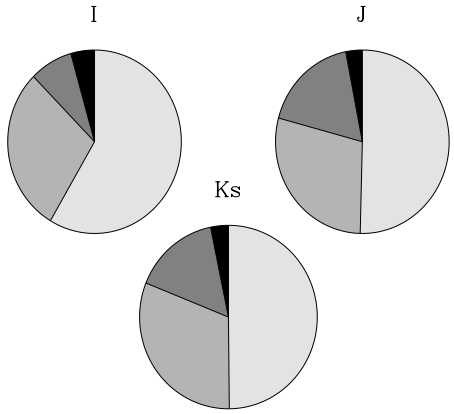

Fig. E-29. Distributions of the DENIS image quality flags for bands I, J and $K_{\rm s}$. The value of the quality flag ranges from 3 (best quality, lightest gray) to 0 (worst quality, darkest gray) in each chart.

4.3. Astrometry

The astrometry is calculated for each image from the present association between I and the USNO_A2 catalogue. Then, the cross associations of J data over I, and of $K_{\rm s}$ data over J are relatively straightforward since all three images have been observed simultaneously. The resulting relative accuracy is better than 0.2" (RMS) in I and 0.4" in J and $K_{\rm s}$. The derived position for I is kept for $I/J/K_{\rm s}$ associations, and the J position is given for the $J/K_{\rm s}$ associated sources. From a comparison made with the TYCHO catalogue in the SgrI field in the Baade's Window, no systematic offset was found. The mean value of the distances was 0.36", with a 0.19" standard deviation (Simon et al., in preparation).

Altogether the present accuracy of the DENIS coordinates used is thus better than 0.5". It will be improved in the future since it is greatly limited by the accuracy of the astrometry of the USNO_A2 catalogue.

4.4. ISOGAL–DENIS cross-identification

The general method that we used to associate DENIS sources with ISOGAL sources is similar to the procedure we used to associate 7 μm and 15 μm data. The only difference arises from the very high density of DENIS sources, so that we used a much smaller association radius, and we cut out the faintest DENIS sources when the source density was too high, in order to reduce the probability of chance associations.

4.4.1. Preliminary selection of DENIS sources

For each ISOGAL field, we used a catalogue of DENIS sources computed by merging the catalogues extracted from the images that overlap the ISO observations. Then, a preliminary selection was done by limiting this catalogue to the true limits of the ISOGAL field, with an additional 20" wide border which was needed because of the uncertainty in the ISO coordinates (see next section). We also only selected the DENIS sources with a K_s detection, since a J–7 μm association without K_s counterpart has a large probability of being a misidentification.

4.4.2. Astrometric correction

As explained in Sect. 4.3, the absolute accuracy of the DENIS coordinates is better than 0.5", thus much better than the ISO astrometry. Therefore we took the DENIS coordinates as the reference system, and computed the global translation offset between the ISOGAL and the DENIS catalogues with the same procedure as for the 7–15 μm associations. The resulting offsets are typically in the range 3–9", as shown in Fig. E-30, and can be explained by the lens wheel jitter of ISOCAM (Sect. 3.6.1). This also implies that the coordinates of ISOGAL sources outside the region with DENIS observations can be wrong by this range of distances.

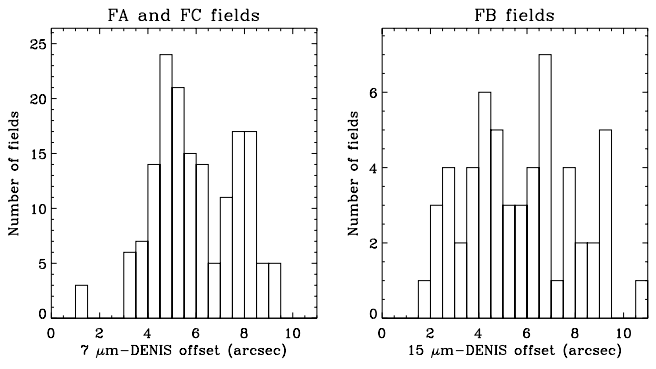

Fig. E-30. Distribution of offset distances between 7 μm and DENIS observations for ISOGAL fields with 7 μm observations (left), and between 15 μm and DENIS observations for ISOGAL fields without 7 μm observations, within the area observed by DENIS.

An approximate polynomial distortion correction was computed with the same procedure as for the 7–15 μm associations, in order to match as best as possible the previous ISO reference coordinates with the DENIS ones. Again, the observed effects were of very small amplitude, but this correction was required to correct for small rotations in the ISOCAM rasters.

4.4.3. Confusion cut of weak DENIS sources

Even after limiting the DENIS catalogue to sources detected at K_s, the density remains very high, exceeding 10^5 sources/deg^2 in the Galactic Centre region. Therefore we further cut the DENIS catalogue to a K_s magnitude that gave a source density of 72 000 sources/deg^2 for the ISO 3" pixel observations. For the observations with 6" pixels, we proceeded in two steps, first limiting the DENIS source density to 18 000 sources/deg^2 and then to 36 000 sources/deg^2 (see below). This confusion cut, with the procedure described below, enabled us to limit the probability of chance associations to a few percent even in the most crowded fields.

4.4.4. Source associations

The search for DENIS associations was done with the same procedure as for the 7–15 μm associations, with a smaller search radius. As shown in Fig. E-31, the mean values of ISO–DENIS separations that we found are typically in the 1–2" range for all ISOGAL fields, with a few larger values for the FB fields, in which the association is done between DENIS and 15 μm coordinates. The corresponding standard deviations are mainly in the 1–1.5" range. An association radius of $\sim$ 3–4" is thus appropriate to find most good associations with a low probability of spurious results. However, a close inspection of the distribution of association radii shows that, in a few fields with poor data quality, a few real associations may have a larger association radius, in particular for blended or extended sources with 6" pixels. Therefore, for the ISO 3"/pixel observations, we used a 3.6" search radius. But for the ISO 6"/pixel observations, we pushed the search up to a radius of 7"; however, we carefully distinguished by quality flags the associations with separations smaller or larger than 3.5".

With such values, the probabilities of random associations given by Eq. (6) may appear high: 23% with 3.6" and a density limit of K_s sources of 72 000 sources/deg^2 used for 3" pixel observations; 5.3 and 11% for 3.5" and 18 000 or 36 000 sources/deg^2, respectively, for 6" pixel; four times these values for 7" search radius. However, as discussed below, because of the large fraction of real associations with smaller separation, the actual fraction of spurious associations with reasonably good quality flags remains much smaller, lower than a few percent. The chance of spurious association is larger for weaker K_s sources al-

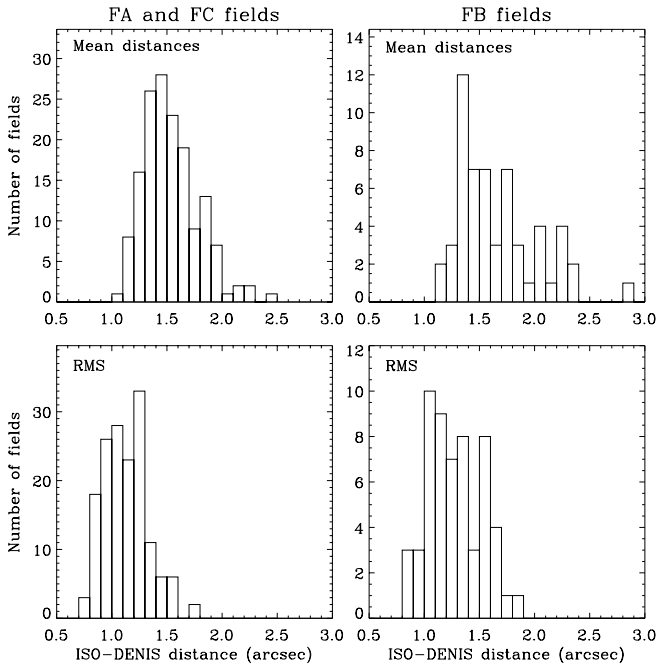

Fig. E-31. *Top panel:* distribution of the mean values of the separations between associated ISOGAL and DENIS sources after astrometric correction in all ISOGAL fields. *Bottom panel:* distribution of the standard deviations of these separations.

lowed with the higher density limit. The final ISO–DENIS quality flag (Sect. 4.4.5) takes this point into account.

4.4.5. The ISO–DENIS association flag

The ISO–DENIS association is also characterised by a specific quality flag, which ranges in values from 5 (highest quality) to 0 and which is computed with the equation:

$$Q_{\rm ID} = 5 - R - N - G - Q$$

where the different terms are defined as follows.

- R, which can take values from 0 to 3, directly depends on the separation d_1 between the ISO source and the associated closest DENIS source. Let $R_{\rm s}$ be half the maximum search radius for the ISO–DENIS association, $R_{\rm s} = 1.8$" for ISO 3" observations and $R_{\rm s} = 3.5$" for ISO 6" observations (as explained in the previous section, a maximum search radius of $2 \times R_{\rm s}$ has been used). We define $R_{\rm c}$ as the root mean square value of the separations of association between ISO and DENIS sources, with the DENIS catalogue limited to a source density of 72 000 sources per square degree for 3" observations, and to 36 000 sources per square degree for 6" observations. Finally, let $R_{\rm m}$ be the minimum between $R_{\rm c}$ and $R_{\rm s}/1.3$. Then, we define R by the following inequalities:
  - if $d_1 \leq R_{\rm m}$ then $R = 0$
  - if $R_{\rm m} < d_1 \leq R_{\rm s}$ then $R = 1$
  - if $R_{\rm s} < d_1 \leq \sqrt{2}R_{\rm s}$ then $R = 2$
  - if $\sqrt{2}R_{\rm s} < d_1 \leq 2R_{\rm s}$ then $R = 3$
- N depends on the number of DENIS sources within the search radius $2 \times R_{\rm s}$. Let d_1 be the distance from the ISO source to the closest DENIS source, d_2 the distance to the second closest source, and $R_{\rm s}$ half the association radius. N is defined as follows:
  - if $d_1 < R_{\rm s}$ and $d_2 > R_{\rm s}$ then $N = 0$
  - if $d_1 < R_{\rm s}$ and $d_2 < R_{\rm s}$ then $N = 1$
  - if $R_{\rm s} \leq d_1 < 2R_{\rm s}$ and $R_{\rm s} \leq d_2 < 2R_{\rm s}$ then $N = 1$
  - if $d_2 > 2R_{\rm s}$ then $N = 0$
- G is relevant only for the ISO 6" observations, it depends on the $K_{\rm s}$ magnitude of the associated DENIS source and it is tailored to trace the actual probability of spurious association. As indicated in Cols. 16 and 17 of the table of ISOGAL fields (see Table 4) two cutoff $K_{\rm s}$ magnitudes K_max1 and K_max2 have been computed to limit the source density of the DENIS catalogue to 18 000 and 36 000 sources per square degree respectively. For ISO sources which are associated with a DENIS source with $K_{\rm s} <$ K_max1, $G = 0$. But for associations with fainter sources with K_max1 $< K_{\rm s} <$ K_max2 (thus with higher DENIS source density) G is set to a positive value, according to the value of g, which is roughly the ratio of the number of new associations with weak $K_{\rm s}$ sources with K_max1 $< K_{\rm s} <$ K_max2, over the number of expected spurious associations with such weak $K_{\rm s}$ sources. For ISOGAL sources with a DENIS association with K_max1 $< K_{\rm s} <$ K_max2, the value of G is set to:
  1 if $g > 5$
  2 if $3 < g \leq 5$
  3 if $2.5 < g \leq 3$
  4 if $2 < g \leq 2.5$
  5 if $g \leq 2$
- Q gives an indication on the global quality of ISO–DENIS associations for each field. From the results of the ISO–DENIS associations, a visual inspection of the histograms of the distances of associations enabled us to derive a global quality flag for each field, which is set to $Q = 0$ when there is no obvious problem, and to $Q = 1$ when there is a significant tail in the distribution of the distances and/or when the RMS of the association distances is greater or roughly equal to R_s (53 fields have $Q = 1$), and to $Q = 2$ when these problems seem more serious (only the FB+02558+00019 field has $Q = 2$).

Let us stress the large fraction of DENIS associations, ∼92% for 7 μm sources, ∼79% for 15 μm sources in FB fields and ∼45% for 15 μm sources with no 7 μm association in FC fields (Fig. 32). The fraction of associations with K_max1 $< K_s <$ K_max2 is also small, ∼4% for 7 μm sources, ∼2.5% for 15 μm sources in FB fields and ∼17% for 15 μm sources with no 7 μm association in FC fields. Therefore, the fraction of spurious associations among accepted associations (see below) always remains small, typically at most ∼1% for 7 μm sources and a few percent for 15 μm sources.

Finally, when the computation of $Q_{\rm ID}$ by the previous formula leads to a negative or null result, the association is considered as invalid, this flag is set to 0 and no DENIS association is given in the catalogue. With this definition, associations with a quality flag equal to 4 or 5 can be considered as secure, while a value of 3 is more uncertain but remains a high probability association, and values of 1 or 2 are more doubtful but still include an appreciable fraction of real associations. The distribution of the computed ISO–DENIS association flags is shown in Fig. 32, where it can be seen that $\sim 87\%$ of the associations found have a good quality (flag ≥ 4), while fewer than 8% of the 7 μm sources (LW2, LW5 and LW6 filters) within the area observed by DENIS have no association.

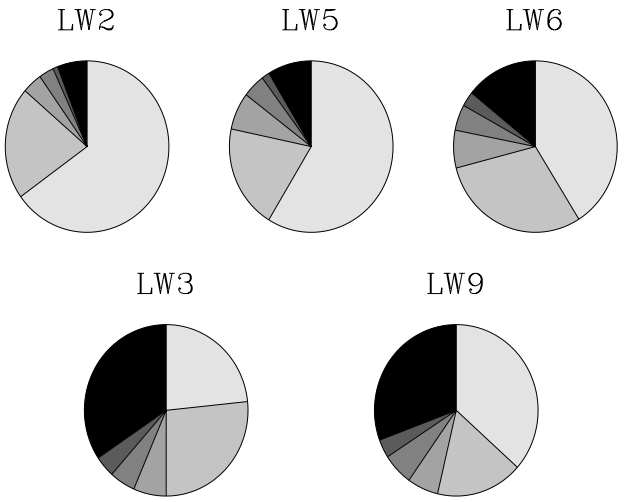

Fig. 32. Distributions of the ISO–DENIS association flag for the different ISO filters. The gray scale corresponds to the different values of this flag, from 5 (lightest gray) to 1 (darkest gray), and the black sectors show the fraction of sources without DENIS association within the area observed by DENIS.

5. ISOGAL–DENIS Point Source Catalogue (version 1)

The Point Source Catalogue contains a total of 106 150 sources, and is composed of two sections. For each field, the "regular" catalogue contains all the sources inside the formal limits of the rectangular field, as defined in Table 4. These limits have been computed to avoid any border effects: all the sources inside this area are located at more than two pixels from the saw-tooth edges of the observed raster, both at 7 and 15 μm for FC fields. This differs from the EDGE flag computed for each wavelength (see Sect. 3.2.5) since the "regular" region is limited to a rectangular area (whose axis are aligned along the galactic ones) which has been fully observed at both wavelengths.

Then, the "edge" catalogue contains the sources outside the limits of the rectangular field, but excluding the measurements at less than two pixels from the saw-tooth edges. This means that in the "edge" region of an FC field, it is possible to find a source with for example a 7 μm detection and no 15 μm counterpart, simply because the edges of the 15 μm raster do not exactly match the ones of the 7 μm raster, so that the source can be outside the region observed at 15 μm or within 2 pixels of one saw-tooth edge. As a result, $\sim$53% of the 7 μm sources and $\sim$81% of the 15 μm sources in the "regular" regions of all FC fields have an association at the other ISO wavelength, while these fractions become $\sim$47% for 7 μm sources and $\sim$70% for 15 μm sources in the "edge" regions.

Both the "regular" and the "edge" catalogues have the format described in Table 16, and a few examples of entries are given in Table 17. The final Catalogue contains 93 385 sources in the "regular" regions, and 12 765 sources in the "edge" regions.

5.1. Position data

The first ten entries for each source in the PSC consist of general data, as described below.

- Col. 1: source number in the field. This number increases with the right ascension of the sources. Each individual catalogue (the "regular" and the "edge" for each field) contains its own numbering, and these numbers are preceded by an "E" in the "edge" catalogues.
- Col. 2: source name. It is composed of 25 characters, following the format:

  $ISOGAL - PJhhmmss.s \pm ddmmssX$

  where "ISOGAL" stands for the ISOGAL–DENIS data, the "P" means that these are provisory data, and the Jhhmmss.s±ddmmss are the J2000 equatorial coordinates of the source, as they appear in Cols. 3 and 4. The last character, 'X', is left blank in all cases but those where two (or exceptionally three) sources from different fields are found at the same position, because they are associated with the same DENIS source and because of edge effects. This concerns 842 sources (0.8% of the PSC) and in all those cases, at least one of the coinciding sources is in an "edge" catalogue. A letter is appended to the name of the sources, starting with an *a* for that in a "regular" catalogue if it exists, otherwise using an arbitrary order between the "edge" catalogues, and going to *b* or *c* when needed.
- Cols. 3 and 4: reference J2000 equatorial coordinates, expressed in decimal degrees. These are the DENIS coordinates when there is a DENIS association (with quality flag $Q_{\rm ID} > 0$), or the ISOGAL corrected to DENIS system coordinates when there is DENIS observation for the field but no DENIS association. Finally, when there is no DENIS observation, these columns give the 7 μm coordinates when they exist, or the 15 μm coordinates corrected to the 7 μm referential for sources in FC field without 7 μm detection, or the 15 μm coordinates for sources in FB fields.

Table 16. Format of the ISOGAL Point Source Catalogue (version 1) - 106 150 entries (see examples in Table 17)

Col.	Name	Format	Units [range]	Description
1	Number	a5		source identification number in the field
2	Name	a25	ISOGAL-PJhhmmss.s±ddmmssX	source identifier (J2000)[a]
3	RAJ2000	f8.4	deg [0–360]	Right Ascension (J2000)[b]
4	DEJ2000	f8.4	deg [-90–+90]	Declination (J2000)
5	RAISOGAL	f8.4	deg [0–360]	ISOGAL RA (J2000)
6	DEISOGAL	f8.4	deg [-90–+90]	ISOGAL Dec (J2000)
7	G_lon	f8.4	deg [-180–+180]	Galactic longitude
8	G_lat	f8.4	deg [-90–+90]	Galactic latitude
9	I_field	a14	Fxsllllsbbbbb	ISOGAL field name
10	D_field	a7		DENIS image name[c]
11	Imag	f5.2	mag	DENIS I-band magnitude[d]
12	Icorr	f4.2	[0–1]	DENIS I-band correlation factor
13	x_I	f5.1	pixel	x-position in DENIS I-band image
14	y_I	f5.1	pixel	y-position in DENIS I-band image
15	Jmag	f5.2	mag	DENIS J-band magnitude[d]
16	Jcorr	f4.2	[0–1]	DENIS J-band correlation factor
17	x_J	f5.1	pixel	x-position in DENIS J-band image
18	y_J	f5.1	pixel	y-position in DENIS J-band image
19	Kmag	f5.2	mag	DENIS K_s-band magnitude[d]
20	Kcorr	f4.2	[0–1]	DENIS K_s-band correlation factor
21	x_K	f5.1	pixel	x-position in DENIS K_s-band image
22	y_K	f5.1	pixel	y-position in DENIS K_s-band image
23	mag7	f5.2	mag	ISOGAL 7 μm magnitude[d]
24	e_mag7	f4.2	mag	uncertainty in 7 μm magnitude
25	filt_7	i1	[2,5,6]	LW number of filter used
26	pfov_7	i1	arcsec [3,6]	pixel field of view
27	x_7	f6.2	pixel	x-position on ISOGAL final 7 μm image
28	y_7	f6.2	pixel	y-position on ISOGAL final 7 μm image
29	npix_7	i1	[0–7]	npix flag at 7 μm (see Sect. 3.2.5)
30	mesh_7	i1	[1,2,3]	mesh flag at 7 μm (see Sect. 3.2.5)
31	edge_7	i1	[0,1]	edge flag at 7 μm (see Sect. 3.2.5)
32	qual_7	i1	[0–4]	global quality flag at 7 μm (see Sect. 3.2.5)
33	mag15	f5.2	mag	ISOGAL 15 μm magnitude[d]
34	e_mag15	f4.2	mag	uncertainty in 15 μm magnitude
35	filt_15	i1	[3,9]	LW number of filter used
36	pfov_15	i1	arcsec [3,6]	pixel field of view
37	x_15	f6.2	pixel	x-position on ISOGAL final 15 μm image
38	y_15	f6.2	pixel	y-position on ISOGAL final 15 μm image
39	npix_15	i1	[0–7]	npix flag at 15 μm (see Sect. 3.2.5)
40	mesh_15	i1	[1,2,3]	mesh flag at 15 μm (see Sect. 3.2.5)
41	edge_15	i1	[0,1]	edge flag at 15 μm (see Sect. 3.2.5)
42	qual_15	i1	[0–4]	global quality flag at 15 μm (see Sect. 3.2.5)
43	dis_II	f5.2	arcsec	separation 7 to 15 μm associated sources
44	ass_II	i1	[0–4]	7–15 μm association quality flag
45	dis_ID	f5.2	arcsec	separation ISOGAL to DENIS associated sources
46	ass_ID	i1	[0–5]	ISOGAL–DENIS association quality flag

[a] The last character 'X' is only present when two sources with the same position have to be distinguished (see text, Sect. 5.1)

[b] Coordinates: the final adopted coordinates (Cols. 3 and 4) are the DENIS ones if there is an association, or the ISO corrected to DENIS if an observation exists but no source was associated. In the northern fields (without DENIS), the coordinates are the 7 μm ones if they exist, or the 15 μm ones for the sources in FB fields, and the 15 μm corrected to 7 μm for the sources detected only at 15 μm in the FC fields. When no DENIS association exists, RAJ2000=RAISOGAL and DEJ2000=DEISOGAL.

[c] Only the seven last digits of the DENIS numbers have been stored, as the three first ones are always 000.

[d] A value of 88.88 for a magnitude means that this position was not observed at this wavelength, while a value of 99.99 means that the source was not detected at this wavelength.

Table 17. Examples of entries in the ISOGAL–DENIS Point Source Catalogue from the C32 field

Col.	Name	Example 1	Example 2	Example 3
1	Number	0008	0017	0007
2	Name	ISOGAL-PJ174118.0-282916	ISOGAL-PJ174122.7-283146	ISOGAL-PJ174117.6-282901
3	RAJ2000	265.3250	265.3446	265.3234
4	DEJ2000	-28.4880	-28.5296	-28.4838
5	RAISOGAL	265.3251	265.3446	265.3230
6	DEISOGAL	-28.4880	-28.5296	-28.4837
7	G_lon	-0.1158	-0.1419	-0.1129
8	G_lat	1.0415	1.0048	1.0449
9	I_field	FC+00000+00100	FC+00000+00100	FC+00000+00100
10	D_field	0955338	0000000	0955339
11	Imag	16.49	99.99	16.36
12	Icorr	0.96	0.0	0.91
13	x_I	367.7	0.0	376.6
14	y_I	153.8	0.0	735.6
15	Jmag	10.87	99.99	10.63
16	Jcorr	0.99	0.0	0.98
17	x_J	369.9	0.0	371.1
18	y_J	154.9	0.0	745.1
19	Kmag	8.32	99.99	8.02
20	Kcorr	0.98	0.0	0.99
21	x_K	368.1	0.0	370.5
22	y_K	151.8	0.0	750.9
23	mag7	7.60	3.47	7.36
24	e_mag7	0.03	0.01	0.03
25	filt_7	2	2	2
26	pfov_7	6	6	6
27	x_7	165.76	181.81	164.10
28	y_7	71.76	50.07	74.02
29	npix_7	2	0	2
30	mesh_7	3	3	3
31	edge_7	0	0	0
32	qual_7	4	4	4
33	mag15	99.99	1.54	5.84
34	e_mag15	0.00	0.03	0.06
35	filt_15	0	3	3
36	pfov_15	0	6	6
37	x_15	0.00	181.64	163.77
38	y_15	0.00	49.86	73.49
39	npix_15	0	1	2
40	mesh_15	0	3	3
41	edge_15	0	0	0
42	qual_15	0	4	4
43	dis_II	0.00	1.06	1.16
44	ass_II	0	4	4
45	dis_ID	0.32	0.00	1.25
46	ass_ID	5	0	5

– Cols. 5 and 6 give the ISOGAL corrected coordinates, which are the ISOGAL extracted coordinates when there is no DENIS observation of the field or the ISOGAL corrected to DENIS system ones when a DENIS observation exists (thus Cols. 3 and 5 as well as Cols. 4 and 6 are identical for sources without DENIS association).
– Cols. 7 and 8 give the galactic reference coordinates corresponding to the reference coordinates given in Cols. 3 and 4, in the commonly used (l^{II}, b^{II}) galactic system.

Table 18. Format of spurious sources Table (version 1)

Col.	Name	Format	Units [range]	Description
1	Number	a4		identification number in the ION
2	RAJ2000	f8.4	deg [0–360]	ISOGAL RA (J2000)
3	DEJ2000	f8.4	deg [-90–+90]	ISOGAL Dec (J2000)
4	Mag	f5.2	mag	ISOGAL magnitude
5	ION	a8		ISO observation number
6	x	f6.2	pixel	x-position on ISOGAL final image
7	y	f6.2	pixel	y-position on ISOGAL final image

– Col. 9 gives the name of the ISOGAL field.
– Col. 10 gives the last seven digits of the number of the DENIS image where an ISO–DENIS association was found. For ISOGAL sources with no DENIS counterpart, this column contains 0000000.

5.2. DENIS data

All the DENIS data are given in Cols. 11 to 22. For each of the three bands, these data are the measured magnitude, the correlation factor with the PSF, and the pixel coordinates of the source in the individual DENIS 12'×12' image, whose reference number is given in Col. 10.

For the ISOGAL sources within the area observed by DENIS but with no DENIS association, the I, J and K_s magnitudes are set to 99.99, while they are set to 88.88 for all the sources located outside the region surveyed by DENIS. In these two cases, the PSF correlation factors and pixel coordinates are set to 0.

The correlation factors with the PSF give an indication of the photometric quality (see Simon et al., in preparation): the uncertainty on the measured magnitude is small when this factor is ≥ 0.95. On the other hand, a value ≤ 0.85 means that the photometry is more uncertain (typically by 0.1 to 0.2 magnitude). For bright sources, this may come from moderate saturation effects, while for faint sources, a value $\leq$0.80 is more typical. Nevertheless, a factor $\leq$0.70 indicates a poor photometric quality, which may be caused by blending effects or confusion with the background.

5.3. ISOCAM data

Cols. 23 to 42 give all the data derived from individual 7 and 15 μm ISO observations, including quality flags (see Sect. 3.2.5), calibrated magnitudes, uncertainties (σ) from the PSF fit measurement of the magnitudes, pixel positions in the final image (after correction of the orientation, see Sect. 7), filter numbers and pixel sizes.

5.4. Association quality flags

The value of the ISOGAL 7–15 μm association flag (see definition in Sect. 3.6.3) is given in Col. 44, and the separation (in arcseconds) between the 7 μm and the 15 μm positions (after correction of the field offset) is given in Col. 43. This flag and the corresponding separation are set to zero for sources with no 7–15 μm association.

For the ISO–DENIS association, the quality flag (see definition in Sect. 4.4.5) is given in Col. 46, and the separation (in arcseconds) between the ISO and the DENIS positions (after correction of the field offset) is given in Col. 45. Again, these two entries are set to zero when there is no ISO–DENIS association.

5.5. Examples

Table 17 shows three examples of entries in the ISOGAL–DENIS Point Source Catalogue. These sources are located in the "C32" field ($l = 0.0$, $b = +1.0$). The first one has been detected at 7 μm but not at 15 μm, and has a DENIS association. The second one has been detected at 7 and 15 μm but has no DENIS association. Finally, the third one is detected in all five bands.

6. Catalogue of spurious sources

As explained in Sect. 3.2.8, three kinds of extracted sources brighter than the limiting magnitude of each field are considered spurious: (1) the sources found only in the 'inversion' processed raster, with no counterpart in a 1 pixel search radius in the 'vision' raster, (2) the sources with simultaneously a doubtful inversion-vision association (with a separation between 0.5 and 1 pixel) and with a poor detection confirmation (i.e. with no association between the $mesh = 1$ and the $mesh = 2$ results), and (3) the possible remnants of bright sources, found by a procedure that looked at the same pixel location in the five successive images of the implied raster.

These sources are published in three distinct tables. Their format is defined in Table 18. The numbers, as they appear in Col. 1, are preceded by an "I" for the "inversion-only" sources, by an "M" for the sources of the second class and by an "R" for the probable remnants.

Note that most spurious sources of the first two kinds are probably artifacts, but can also be related to faint extended structures, for which different parameters in the extraction process result in slightly different coordinates. The third class of spurious sources is essentially composed of spurious remnants, but may contain a few real sources,

which have been accidentally discarded by the procedure because of spatial coincidence with a putative remnant.

7. ISOCAM corrected images

The ISOCAM images have been initially processed using version 7.0 of the off-line processing pipeline (Sect. 3.1). Similar images processed with the latest version of OLP are now publically available through the Data Archive on the ISO web site[4]. However, we make available here the OLP7 images together with version 1 of the PSC for consistency, because they have been used for the extraction of the sources of this catalogue. Improved ISOGAL images (Miville-Deschênes et al. 2000 and in preparation) will be published with version 2 of the catalogue.

Because of the difference in orientation between the individual images (aligned along the satellite axis, thus with the equatorial coordinates) and the mosaiced rasters (aligned along the galactic axes), and of different times of observations, the orientation obtained after the OLP7 processing was different from one raster to another. We therefore decided to change this orientation if necessary, in order to use the same convention for all rasters, and set the orientation to l along decreasing X and b along increasing Y.

A more important improvement provided by the construction of the ISOGAL PSC deals with the astrometry, which has been tied to DENIS whenever possible. The offsets that we applied to the source coordinates in order to associate the ISO sources with DENIS have also been applied to the rasters, as indicated in Table 2. For the FC fields with no DENIS observation, the astrometry of the 15 μm rasters has been tied to that of the 7 μm ones. The corrected images are available through the CDS and the IAP[5] server.

8. Summary

The first version of the ISOGAL–DENIS Point Source Catalogue contains a total of 106 000 sources, with one or two magnitude measurements in the mid-infrared (7 and 15 μm), and up to three magnitude measurements in the near-infrared (I, J and K_s bands of the DENIS survey, see Table 16 and Table 17). The data are presented in two similar tables, corresponding to the "regular" and the "edge" regions of the observed fields. The latter contains the sources from the edges of the ISOCAM rasters, where border effects can occur, which can lead to non-association between the two ISO bands.

The typical RMS photometric uncertainty is at most ∼0.1 mag for the DENIS bands, and better than 0.15 mag for the ISO bands in most cases, but it can reach 0.3 mag for the faintest sources in the densest fields. For the most numerous fields observed with broad filters, the limiting magnitudes of the published catalogues range between 8.8 and 10.1 at 7 μm (with a median value equal to 9.46 mag, or $F_\nu \sim 15$ mJy), and between 7.7 and 8.8 at 15 μm (median 8.16 mag, $F_\nu \sim 11$ mJy), depending on the source density. For the most difficult fields observed with narrow filters, these limits range between 8.2 and 9.6 mag at 7 μm and between 7.0 and 8.2 mag at 15 μm. These limits are conservative and the fainter sources have been rejected in the present version of the PSC[6].

The current astrometric accuracy of the DENIS data used is better than 0.5" (RMS). The final coordinates (as they appear in Cols. 3 and 4 of the catalogue - see Table 16 - in equatorial J2000 system, in Cols. 7 and 8 in the galactic system, and in the name of the source, Col. 2) of all ISOGAL sources with a DENIS counterpart are the DENIS ones, and should also be accurate to 0.5". The astrometry of the ISOGAL sources with no DENIS association, but within the fields observed by DENIS, is also tied to the DENIS coordinates, and should therefore be accurate to ∼2" (RMS, see Fig. E-31). Finally, ISOGAL sources located outside the area surveyed by DENIS may suffer from the lens wheel jitter of ISOCAM, resulting in a maximum ∼10" systematic offset in the extracted coordinates.

Several flags have been implemented to characterise the reliability of the sources, the quality of their photometry and of the associations between the different bands. An indication of the reliability of the mid-infrared detection is also given by the *mesh* flag (Col. 30 for 7 μm and Col. 40 for 15 μm, see Table 16). A value of 3 indicates a good reliability level, while a value of 1 or 2 shows that the extraction was not perfectly confirmed, making the real point-like nature of the source doubtful.

The global quality of the ISO photometry and reliability of each source is quantified by one quality flag for each band. These two flags are given in Col. 32 for 7 μm and in Col. 42 for 15 μm, and range from 1 to 4, the highest value corresponding to the best quality. Thus sources with quality flags equal to 1 or 2 should be considered with caution.

The quality of the association between the two ISO bands is also characterised by a specific flag, which appears in Col. 44, together with the separation of the association in Col. 43. When this flag is equal to 3 or 4, which means that the separation between the 7 μm coordinates and the 15 μm ones is smaller than one pixel, the validity of the association is almost certain, while a value of 1 or 2 means that the association has to be carefully checked, but it may be a real association for slightly extended sources.

Finally, the quality of the ISO–DENIS association is quantified by a flag given in Col. 46 (and the ISO–DENIS separation appears in Col. 45). Here, values of 4 or 5 correspond to secure associations, while a value of 3 means that the association was not straightforward, but it still has a good probability to be real. When this flag is equal

[4] http://www.iso.vilspa.esa.es/ida/index.html
[5] http://www-isogal.iap.fr/Fields/index_tdt.html

[6] The complete catalogues, including the faint sources rejected, may be obtained by requesting the ISOGAL PI, omont@iap.fr

to 1 or 2, the reality of the association has to be checked carefully, using for instance colour compatibility criteria.

9. Conclusion

With the first public version of the ISOGAL–DENIS Point Source Catalogue, we provide the astronomical community with a catalogue containing about 10^5 mid-infrared sources, detected at 7 and/or 15 μm in the obscured centre of the Galaxy. The bulk of them are associated with near-infrared data from the DENIS survey. We also provide nearly 400 mid-infrared images, with an astrometric accuracy of $\sim$1" for most of them.

All the data were reduced using data products of version 7 of the ISO off-line processing pipeline. Additional specific procedures enabled us to greatly reduce the number of artifacts and to reduce the photometric uncertainty to typically 0.15 mag, at the cost of limiting the published catalogue in the densest observed fields to levels well above the sensitivity limit of a few mJy.

A second version of the catalogue is already under development, based on a systematic reprocessing of the raw data using the most up-to-date specialised procedures (Miville-Deschênes 2000 and in preparation). This second version will also contain systematic cross-associations with the near-infrared data of the 2MASS survey, and with the mid-infrared data of the MSX survey.

Acknowledgements. We thank the whole ISOGAL Team for its contribution to the project and to the production of the present catalogue.

The ISOCAM data presented in this paper were analysed using 'CIA', a joint development by the ESA Astrophysics Division and the ISOCAM Consortium. The ISOCAM Consortium is led by the ISOCAM PI, C. Cesarsky. We thank A. Abergel, H. Aussel, A. Coulais, R. Gastaud, M. Pérault, J.L. Starck and many other members of the ISOCAM team, of the ISO/ESA team at Villafranca and especially of the CIA team for their help in the ISOGAL data reduction. We are very grateful to all people who contributed to the ISOGAL data reduction, including T. August, X. Bertou, E. Copet and M. Unavane.

We thank the whole DENIS Team, and especially its PI, N. Epchtein, and S. Bégon, J. Borsenberger, B. de Batz, P. Fouqué, S. Kineswenger & D. Tiphène for making available the DENIS data. The DENIS project is supported, in France by the Institut National des Sciences de l'Univers, the Education Ministry and the Centre National de la Recherche Scientifique, in Germany by the State of Baden-Würtemberg, in Spain by the DGICYT, in Italy by the Consiglio Nazionale delle Ricerche, in Austria by the Fonds zur Förderung der wissenschaftlichen Forschung and the Bundesministerium für Wissenschaft und Forschung.

This publication made use of data products from the Midcourse Space Experiment. Processing of the data was funded by the Ballistic Missile Defense Organization with additional support from NASA Office of Space Science.

This work was carried out in the context of EARA, the European Association for Research in Astronomy.

S. Ganesh was supported by a fellowship from the Ministère des Affaires Etrangères, France, and this research was supported by the Project 1910-1 of Indo-French Center for the Promotion of Advanced Research (CEFIPRA). SG also acknowledges the support he received from the French CNRS for participating in the astronomical school in Les Houches in 1998. M. Schultheis acknowledges the receipt of an ESA fellowship. B. Aracil and A. Soive were posted to the ISOGAL Project by the Délegation Générale de l'Armement, France.

We are grateful to Dr. M. Cohen for his help in the calibration of ISOCAM data, and to Dr. S. Ott and Prof. I.S. Glass for their useful comments and inputs.

References

Abergel, A., Miville-Deschênes, M.-A., Désert, F.-X., et al. 1998, "The transient behaviour of the long wavelength channel of ISOCAM", http://www.iso.vilspa.esa.es/users/expl_lib/CAM/transient_detector_ws.ps.gz

Aussel, H. 1998, August 13, "ISOCAM LW channel Field of View Distortion", http://www.iso.vilspa.esa.es/users/expl_lib/CAM/distortion.ps.gz

Bellazzini, M., Fusi Pecci, F., Montegriffo, P., et al. 2002, AJ 123, 2541

Biviano, A., Sauvage, M., Gallais, P., et al. 1998, May 18, "The ISOCAM Dark Current Calibration Report", http://www.iso.vilspa.esa.es/users/expl_lib/CAM/darkdoc.ps.gz

Blommaert, J. A. D. L. 1998, December 18, "ISOCAM Photometry Report", http://www.iso.vilspa.esa.es/users/expl_lib/CAM/photom_rep_fn.ps.gz

Blommaert, J. A. D. L., Metcalfe, L., Altieri, B., et al. 2000, Experimental Astronomy 10, 241

Blommaert, J. A. D. L., Siebenmorgen, R., Coulais, A., et al. 2001, "The ISO Handbook, Volume III: CAM - The ISO Camera", http://www.iso.vilspa.esa.es/manuals/HANDBOOK/III/cam_hb/

Bontemps, S., André, P., Kaas, A. A., et al. 2001, A&A 372, 173

Burgdorf, M. J., Cohen, M., Price, S. D., et al. 2000, A&A 360, 111

Cesarsky, C. J., Abergel, A., Agnèse, P., et al. 1996, A&A 315, L32

Coulais, A., & Abergel, A. 2000, A&AS 141, 533

Dole, H., Gispert, R., Lagache, G., et al. 2001, A&A 372, 364

Egan, M. P., Shipman, R. F., Price, S. D., et al. 1998, ApJ 494, L199

Elbaz, D., Cesarsky, C. J., Fadda, D., et al. 1999, A&A 351, 37

Epchtein, N., de Batz, B., Copet, E., et al. 1994, Ap&SS 217, 3

Epchtein, N., de Batz, B., Capoani, L., et al. 1997, The Messenger 87, 27

Felli, M., Comoretto, G., Testi, L., Omont, A., & Schuller, F. 2000, A&A 362, 199

Felli, M., Testi, L., Schuller, F., & Omont, A. 2002, A&A 392, 971

Fouqué, P., Chevallier, L., Cohen, M., et al. 2000, A&AS 141, 313

Glass, I. S., Ganesh, S., Alard, C., et al. 1999, MNRAS 308, 127

Hammersley, P. L., Jourdain de Muizon, M., Kessler, M. F., et al. 1998, A&AS 128, 207

Hennebelle, P., Pérault, M., Teyssier, D., & Ganesh, S. 2001, A&A 365, 598

Jiang B. W., Omont A., Ganesh S., Simon G., Schuller F. 2003, A&A 400, 903
Kessler, M. F., Steinz, J. A., Anderegg, M. E., et al. 1996, A&A 315, L27
Lumsden, S. L., Hoare, M. G., Oudmaijer, R. D., & Richards, D. 2002, MNRAS 336, 621
Mill, J. D., O'Neil, R. R., Price, S., et al. 1994, Journal of Spacecraft and Rockets 31, 900
Miville-Deschênes, M.-A., Boulanger, F., Abergel, A., & Bernard, J.-P. 2000, A&AS 146, 519
Nordh, L., Olofsson, G., Bontemps, S., et al. 1998, in ASP Conf. Ser. 132, Star Formation with the Infrared Space Observatory, ed. J. Yun & R. Liseau, 127
Ojha D. K., Omont A., Schuller F., et al. 2003, A&A 403, 141
Omont, A., Ganesh, S., Alard, C., et al. 1999, A&A 348, 755
Omont, A., Gilmore, G. F., Alard, C., et al. 2003, A&A, this issue
Ortiz, R., Blommaert, J. A. D. L., Copet, E., et al. 2002, A&A 388, 279
Ott, S., Abergel, A., Altieri, B., et al. 1997, Design and Implementation of CIA, the ISOCAM Interactive Analysis System. In ASP Conf. Ser. 125, ed. G. Hunt & H. E. Payne, 34
Ott, S. 2002, PhD Thesis, Paris VI - Pierre et Marie Curie University
Pérault, M., Omont, A., Simon, G., et al. 1996, A&A 315, L165
Price, S. D., Egan, M. P., Carey, S. J., Mizuno, D. R., & Kuchar, T. A. 2001, AJ 121, 2819
Rowan-Robinson, M., Oliver, S., Efstathiou, A., et al. 1999, in The Universe as Seen by ISO, ed. P. Cox & M. F. Kessler., ESA-SP 427, 1011
Schuller, F. 2002, PhD Thesis, Paris VI - Pierre et Marie Curie University
Schultheis, M., Ganesh, S., Glass, I. S., et al. 2000, A&A 362, 215
Skrutskie, M. F., Schneider, S. E., Stiening, R., et al. 1997, in The Impact of Large Scale Near-IR Sky Surveys, ed. F. Garzon, N. Epchtein, A. Omont et al. (Dordrecht: Kluwer), 25
Starck, J.-L. 1998, in Les Houches Summer School on 'Infrared Astronomy from Space: Today and Tomorrow'
Starck, J.-L., Murtagh, F., & Bijaoui, A. 1998, *Image Processing and Data Analysis: The Multiscale Approach*, Cambridge University Press
Testi, L., Felli, M., Omont, A., et al. 1997, A&A 318, L13
Zavagno, A., & Ducci, V. 2001, A&A 371, 312

APPENDIX A - The 263 ISOGAL fields

Table A-1: Catalogue of ISOGAL FA (7 μm) fields

Field name	ISO obs. number	LW filter	Pixel size (")	l_0 (°)	b_0 (°)	dl (°)	db (°)
FA–06005–00075	60900367	2	6	-60.0395	-0.7511	0.0773	0.1439
FA–05187–00002	63003361	2	6	-51.8693	-0.0202	0.0872	0.2479
FA–05185–00080	63003363	2	6	-51.8481	-0.8009	0.0996	0.1441
FA–05184+00075	63003360	2	6	-51.8394	0.7500	0.0870	0.1643
FA–04519+00071	60600457	2	6	-45.1868	0.7117	0.0996	0.1645
FA–04500–00076	60600459	2	6	-44.9974	-0.7572	0.0885	0.1441
FA–03700–00073	48800856	2	6	-36.9990	-0.7298	0.0975	0.1412
FA–03689+00073	48800853	2	6	-36.8897	0.7304	0.0877	0.1433
FA–03003+00071	47401449	2	6	-30.0278	0.7120	0.0861	0.1428
FA–02987+00042	48401051	2	6	-29.8707	0.4107	0.1869	0.1372
FA–02976–00077	47401452	2	6	-29.7586	-0.7681	0.0858	0.1431
FA–02599–00079	48401248	2	6	-25.9897	-0.7892	0.0857	0.1425
FA–02583+00072	48401244	2	6	-25.8296	0.7209	0.0881	0.1440
FA–02410–00005	47401572	2	6	-24.0978	-0.0485	0.0469	0.1858
FA–02221–00076	49001343	2	6	-22.2076	-0.7581	0.0861	0.1428
FA–02218+00070	49001238	2	6	-22.1779	0.7016	0.0877	0.1438
FA–01887+00072	48801333	2	6	-18.8709	0.7203	0.0882	0.1441
FA–01869–00075	48801637	2	6	-18.6906	-0.7496	0.0854	0.1424
FA–01534+00010	48801431	2	6	-15.3415	0.1005	0.1866	0.1079
FA–01531+00073	48801529	2	6	-15.3109	0.7303	0.0883	0.1440
FA–01523–00074	48801532	2	6	-15.2308	-0.7398	0.0855	0.1424
FA–01244+00078	48401325	2	6	-12.4398	0.7807	0.0870	0.1434
FA–01226–00074	48401328	2	6	-12.2500	-0.7393	0.0869	0.1433
FA–00999–00072	64801324	2	6	-9.9900	-0.7193	0.0863	0.1443
FA–00990+00072	64801322	2	6	-9.9001	0.7204	0.0865	0.1444
FA–00739–00072	50501821	2	6	-7.3880	-0.7185	0.0868	0.1432
FA–00737+00078	50501816	2	6	-7.3681	0.7818	0.0877	0.1438
FA–00076+00019	49800123	6	6	-0.7595	0.1849	0.0385	0.0729
FA–00047–00006	31300236	5	3	-0.4730	-0.0549	0.0420	0.1441
FA–00006+00296	83701130	2	6	-0.0602	2.9601	0.0466	0.1426
FA–00005+00400	83701032	2	6	-0.0507	3.9999	0.0455	0.1422
FA–00005+00204	83701253	2	6	-0.0505	2.0503	0.0477	0.1430
FA+00000+00600	83700534	2	6	-0.0004	5.9999	0.0436	0.1414
FA+00580+00076	48700809	2	6	5.7994	0.7610	0.0879	0.1439
FA+00712+00068	48700615	2	6	7.1219	0.6825	0.0880	0.1439
FA+00737–00070	47700720	2	6	7.3720	-0.6986	0.0865	0.1431
FA+01010+00020	49300923	2	6	10.1016	0.1990	0.0487	0.0810
FA+01211–00076	49300131	2	6	12.1112	-0.7589	0.0870	0.1433
FA+01211+00066	49300126	2	6	12.1114	0.6617	0.0880	0.1439
FA+02232–00069	47200752	2	6	22.3224	-0.6883	0.0877	0.1432
FA+02577+00076	47201153	2	6	25.7715	0.7614	0.0891	0.1436
FA+02577–00065	48100559	2	6	25.7724	-0.6485	0.1005	0.1021
FA+06750+00074	73300136	2	6	67.4999	0.7408	0.0864	0.1443

Table A-2: Catalogue of ISOGAL FB (15 μm) fields

Field name	ISO obs. number	LW filter	Pixel size (")	l_0 (°)	b_0 (°)	dl (°)	db (°)
FB–04522+00015	24901254	3	6	-45.2160	0.1470	0.1610	0.3522
FB–04522–00044	24901254	3	6	-45.2160	-0.4391	0.1610	0.0564
FB–04513–00028	24901254	3	6	-45.1330	-0.2939	0.0780	0.0887
FB–03015+00012	31500852	3	6	-30.1397	0.1149	0.0747	0.1508
FB–03001–00010	31500852	3	6	-30.0002	-0.1026	0.2142	0.0666
FB–02581–00005	08700645	3	6	-25.8108	-0.0505	0.1090	0.2069
FB–02547–00033	31500348	3	6	-25.4804	-0.3218	0.0952	0.1694

Table A-2: Catalogue of ISOGAL FB fields (continued)

Field name	ISO obs. number	LW filter	Pixel size (")	l_0 (°)	b_0 (°)	dl (°)	db (°)
FB–02219+00011	31500440	3	6	-22.1904	0.1033	0.0750	0.1235
FB–01545–00022	31100231	3	6	-15.4504	-0.2204	0.1618	0.1416
FB–01258+00025	31100326	3	6	-12.5816	0.2446	0.0883	0.2603
FB–00966+00005	31100123	3	6	-9.6639	0.0500	0.0801	0.2469
FB–00576+00004	31500512	3	6	-5.7598	0.0391	0.1372	0.0418
FB–00436–00003	31100504	3	6	-4.3609	-0.0297	0.1218	0.4773
FB–00416–00007	31100505	3	6	-4.1632	-0.0702	0.0638	0.1011
FB–00367–00105	50501669	3	6	-3.6679	-1.0482	0.0726	0.1635
FB–00289–00016	31100401	3	6	-2.8891	-0.1524	0.2259	0.0777
FB–00115–00076	31301047	3	6	-1.1596	-0.7607	0.1503	0.0800
FB–00081–00035	31300313	9	6	-0.8162	-0.3483	0.0578	0.1744
FB–00075–00100	50501503	9	6	-0.7488	-0.9984	0.0882	0.0816
FB–00075+00100	49800101	9	6	-0.7487	1.0010	0.0868	0.0800
FB–00057+00040	31801220	9	6	-0.5755	0.3890	0.2225	0.1189
FB–00042–00040	31300314	9	6	-0.4202	-0.3998	0.0678	0.1004
FB–00008+00074	50502013	3	6	-0.0775	0.7453	0.1487	0.1991
FB–00006–00204	50501515	3	6	-0.0583	-2.0484	0.0740	0.1641
FB–00006–00318	50501516	3	6	-0.0580	-3.1782	0.0723	0.1633
FB–00001+00018	31300901	9	6	-0.0107	0.1776	0.0463	0.0768
FB+00009+00194	49800113	3	6	0.0923	1.9415	0.0725	0.1633
FB+00018+00085	31801312	3	6	0.1748	0.8498	0.0959	0.0587
FB+00032+00217	32500240	3	6	0.3225	2.1709	0.1448	0.0483
FB+00075–00100	49701604	9	6	0.7483	-1.0003	0.0879	0.0812
FB+00075+00100	49800202	9	6	0.7510	1.0017	0.0875	0.0807
FB+00089+00017	32500152	9	6	0.8928	0.1708	0.1508	0.0889
FB+00095+00038	32500116	9	6	0.9525	0.3804	0.1125	0.1207
FB+00141–00100	32500341	3	6	1.4132	-0.9986	0.0647	0.0456
FB+00363–00105	47001186	3	6	3.6294	-1.0505	0.0756	0.1640
FB+00369+00095	47001285	3	6	3.6890	0.9495	0.0737	0.1632
FB+00397+00027	14100107	3	6	3.9737	0.2703	0.0852	0.1631
FB+00416–00009	14100106	3	6	4.1606	-0.0893	0.1073	0.1012
FB+00548+00007	13800111	3	6	5.4814	0.0695	0.1985	0.1221
FB+00986+00040	13800421	3	6	9.8575	0.3967	0.1879	0.1075
FB+01185–00042	13800524	3	6	11.8542	-0.4211	0.0498	0.0786
FB+01244+00010	13800626	3	6	12.4388	0.0982	0.1127	0.0730
FB+01506–00035	13801129	3	6	15.0610	-0.3449	0.1259	0.0765
FB+01814+00007	13801538	3	6	18.1479	0.0695	0.0480	0.1013
FB+01829+00015	13801538	3	6	18.2860	0.1507	0.0901	0.0202
FB+01830–00014	13801561	3	6	18.3087	-0.1408	0.0505	0.1028
FB+01857–00042	13801534	3	6	18.5689	-0.4182	0.0616	0.0989
FB+01870+00037	13801637	3	6	18.6972	0.3634	0.0353	0.1421
FB+01917–00004	13801562	3	6	19.1682	-0.0383	0.0487	0.0433
FB+02230+00008	13801742	3	6	22.2984	0.0784	0.0495	0.0549
FB+02238–00003	13801742	3	6	22.3811	-0.0228	0.1366	0.0464
FB+02558+00019	13801947	3	6	25.5790	0.1855	0.0753	0.0457
FB+02562–00047	13801945	3	6	25.6189	-0.4626	0.0750	0.0323
FB+03007+00033	13901253	3	6	30.0663	0.3323	0.0775	0.1854
FB+03013+00005	13901252	3	6	30.1319	0.0542	0.0623	0.0848
FB+03038+00001	13901354	3	6	30.3811	0.0103	0.0610	0.0705
FB+03038+00036	13901354	3	6	30.3811	0.3626	0.0610	0.0613

Table A-3: Catalogue of ISOGAL FC (7+15 μm) fields

Field name	ISO 7 μm obs. num.	ISO 15 μm obs. num.	7 μm filter	15 μm filter	Pixel size (")	l_0 (°)	b_0 (°)	dl (°)	db (°)
FC–07940-03232	77500315	77500316	2	3	6	-79.4025	-32.3088	0.0436	0.0629
FC–05980+00016	60900365	60900366	2	3	6	-59.7969	0.1602	0.1234	0.1841
FC–05410-04489	78900220	78900221	2	3	3	-54.1026	-44.8898	0.0115	0.0130

Table A-3: Catalogue of ISOGAL FC fields (continued)

Field name	ISO 7 μm obs. num.	ISO 15 μm obs. num.	7 μm filter	15 μm filter	Pixel size (")	l_0 (°)	b_0 (°)	dl (°)	db (°)
FC–04530–00028	24901259	24901254	2	3	6	-45.2959	-0.2925	0.0797	0.0788
FC–04496+00000	24901257	60600458	2	3	6	-44.9606	0.0027	0.0816	0.4974
FC–03668–00001	48800854	48800855	2	3	6	-36.6818	-0.0101	0.0790	0.3288
FC–03011–00034	47401450	08700751	2	3	6	-30.1095	-0.3412	0.1860	0.1628
FC–02992+00012	48401051	31500852	2	3	6	-29.9218	0.1178	0.1358	0.1480
FC–02584+00038	48401246	31500347	2	3	6	-25.8396	0.3785	0.1882	0.1213
FC–02547+00000	48401247	31500348	2	3	6	-25.4804	0.0011	0.0952	0.1425
FC–02219–00013	49001240	31500440	2	3	6	-22.1889	-0.1268	0.0735	0.1007
FC–02194–00033	49001241	08700441	2	3	6	-21.9417	-0.3284	0.1747	0.0589
FC–02190+00005	49001239	08700544	6	3	6	-21.9003	0.0516	0.0709	0.2676
FC–01904+00013	48801334	31500234	2	3	6	-19.0380	0.1297	0.0694	0.3736
FC–01873–00003	48801335	31500235	2	3	6	-18.7398	-0.0295	0.0990	0.1431
FC–01863+00035	48801636	31500236	2	3	6	-18.6298	0.3499	0.1747	0.1423
FC–01534+00037	48801431	31100233	2	3	6	-15.3415	0.3597	0.1866	0.1424
FC–01258–00015	48401327	31100326	2	3	6	-12.5816	-0.1575	0.0883	0.1338
FC–01236–00040	48401326	31100324	2	3	6	-12.3595	-0.4004	0.2252	0.1005
FC–00980+00005	64801323	31100123	2	3	6	-9.8004	0.0500	0.0502	0.2469
FC–00785+00001	64801219	64801220	2	3	6	-7.8510	0.0100	0.0616	0.4154
FC–00724–00023	50501817	50501818	2	3	6	-7.2382	-0.2280	0.0621	0.1434
FC–00603+00001	49100913	31500511	2	3	6	-6.0250	0.0096	0.1229	0.1631
FC–00576+00017	49100914	31500512	2	3	6	-5.7598	0.1656	0.1372	0.0753
FC–00575–00023	49100912	31500510	2	3	6	-5.7491	-0.2303	0.1369	0.0801
FC–00566+00070	49100911	84000428	2	3	6	-5.6579	0.7023	0.0861	0.1428
FC–00536–00081	49100915	84000429	2	3	6	-5.3581	-0.8075	0.0865	0.1433
FC–00429–00075	50501610	84000327	2	3	6	-4.2870	-0.7487	0.0728	0.1638
FC–00428+00079	50601207	84000326	2	3	6	-4.2776	0.7924	0.0872	0.1435
FC–00289+00016	50701205	31100401	2	3	6	-2.8870	0.1613	0.1498	0.2268
FC–00272+00069	49701702	49701770	2	3	6	-2.7216	0.6893	0.0867	0.1639
FC–00272–00074	50601306	50601371	2	3	6	-2.7184	-0.7377	0.0876	0.1436
FC–00170+00034	49701701	31900202	2	3	6	-1.7006	0.3393	0.0979	0.1621
FC–00149+00100	83701309	32500238	2	3	6	-1.4897	1.0008	0.1432	0.0479
FC–00149–00100	83801111	32500342	2	3	6	-1.4893	-1.0002	0.1428	0.0464
FC–00121–00003	31300837	84101058	5	9	6	-1.2147	-0.0309	0.0736	0.1429
FC–00112–00035	84300224	31300313	6	9	6	-1.1205	-0.3439	0.2358	0.1700
FC–00109+00031	50501430	31801219	6	9	6	-1.0890	0.3061	0.2824	0.1941
FC–00100–00600	84001336	84001337	2	3	6	-1.0006	-6.0002	0.0429	0.1424
FC–00090–00003	31300837	83800857	5	9	6	-0.8959	-0.0309	0.1709	0.1429
FC–00062–00006	31300236	83600308	5	9	3	-0.6205	-0.0534	0.0985	0.1426
FC–00062–00040	84300225	84100738	6	9	6	-0.6198	-0.3997	0.1242	0.1016
FC–00039+00018	49800123	31300901	6	9	6	-0.3878	0.1788	0.3268	0.0756
FC–00027–00006	31300135	82700140	5	9	3	-0.2695	-0.0523	0.1547	0.1416
FC+00000+00100	83600418	83600523	2	3	6	-0.0011	0.9990	0.1441	0.0471
FC+00000–00100	84100926	84100927	2	3	6	-0.0011	-1.0013	0.1447	0.0488
FC+00004+00040	49702229	13600318	6	9	6	0.0408	0.3892	0.3866	0.1190
FC+00005–00024	83600855	83600856	5	9	6	0.0532	-0.2384	0.1494	0.1226
FC+00032–00217	84100428	84100429	2	3	6	0.3190	-2.1717	0.1442	0.0469
FC+00034–00005	31300734	82800341	5	9	3	0.3456	-0.0500	0.1171	0.1325
FC+00037+00017	84100143	13600503	5	9	6	0.3702	0.1696	0.2872	0.0796
FC+00059+00002	31300433	83800712	5	9	3	0.5934	0.0254	0.1197	0.0571
FC+00062–00014	31300433	84100259	5	9	3	0.6197	-0.1399	0.1054	0.0510
FC+00066–00041	47601120	47601119	6	9	6	0.6642	-0.4078	0.3827	0.1020
FC+00067+00038	49702227	32500116	6	9	6	0.6683	0.3804	0.1624	0.1207
FC+00089–00009	49800226	32500152	6	9	6	0.8928	-0.0889	0.1508	0.1648
FC+00103–00383	84001115	84001116	2	3	6	1.0287	-3.8304	0.1083	0.1197
FC+00113–00417	84001222	84001223	2	3	3	1.1425	-4.1655	0.0363	0.0445
FC+00124–00032	49701618	49701617	6	9	6	1.2382	-0.3298	0.1877	0.1845
FC+00127+00035	49800228	32500117	6	9	6	1.2719	0.3503	0.1875	0.1636
FC+00137–00263	83800913	83800914	2	3	6	1.3695	-2.6304	0.1099	0.1205
FC+00149+00100	84001007	32500239	6	3	6	1.4903	0.9999	0.1427	0.0473

Table A-3: Catalogue of ISOGAL FC fields (continued)

Field name	ISO 7 μm obs. num.	ISO 15 μm obs. num.	7 μm filter	15 μm filter	Pixel size (")	l_0 (°)	b_0 (°)	dl (°)	db (°)
FC+00163–00100	84101405	84101406	6	9	6	1.6286	-1.0009	0.1435	0.0453
FC+00192–00012	47001889	31900116	6	3	6	1.9191	-0.1206	0.0990	0.2886
FC+00269+00013	67700402	47001503	2	3	6	2.6895	0.1300	0.1497	0.1425
FC+00270–00070	47001504	47001588	2	3	6	2.6988	-0.6996	0.0864	0.1422
FC+00280+00074	67700401	67700487	2	3	6	2.7995	0.7408	0.0880	0.1432
FC+00282–00029	84901044	14100101	6	3	6	2.8217	-0.2889	0.0731	0.2056
FC+00419+00027	47001107	14100107	2	3	6	4.1890	0.2703	0.1245	0.1631
FC+00434–00069	47001108	87200535	2	3	6	4.3514	-0.6895	0.0986	0.1222
FC+00440–00009	47001206	14100106	2	3	6	4.3995	-0.0906	0.1256	0.0813
FC+00442+00067	47001205	87200534	2	3	6	4.4200	0.6715	0.0859	0.1425
FC+00525–00302	84001724	84001725	2	3	3	5.2524	-3.0192	0.0414	0.0502
FC+00552+00045	48700813	13800212	2	3	6	5.5196	0.4503	0.1751	0.0596
FC+00567–00028	48700811	13800210	2	3	6	5.6692	-0.2898	0.0877	0.1647
FC+00581+00014	48700810	13800109	2	3	6	5.8097	0.1346	0.1244	0.1801
FC+00597–00076	48700814	87200637	2	3	6	5.9703	-0.7593	0.1113	0.1216
FC+00733+00015	48700616	48700617	2	3	6	7.3323	0.1512	0.0994	0.1634
FC+00760–00023	47700718	47700719	2	3	6	7.6025	-0.2288	0.0987	0.1840
FC+00955–00009	83400901	13800323	2	3	6	9.5518	-0.0884	0.1380	0.2174
FC+00975–00074	49301525	87200741	2	3	6	9.7514	-0.7385	0.0878	0.1431
FC+00976+00067	49300921	87200740	2	3	6	9.7599	0.6711	0.0864	0.1426
FC+00985–00020	49301522	13800420	2	3	6	9.8539	-0.2008	0.1494	0.2051
FC+00986+00021	49300923	13800421	2	3	6	9.8575	0.2075	0.1879	0.0725
FC+01205+00025	46700630	13800527	2	3	6	12.0487	0.2495	0.2379	0.0798
FC+01206–00042	49300127	13800524	2	3	6	12.0621	-0.4211	0.1503	0.0786
FC+01239–00021	46700628	13800625	2	3	6	12.3895	-0.2092	0.0989	0.2263
FC+01496–00014	87200203	13801130	6	3	6	14.9604	-0.1400	0.0854	0.1215
FC+01508+00012	87200205	13801108	6	3	6	15.0810	0.1184	0.0489	0.1278
FC+01509–00007	87200205	13801108	6	3	6	15.0914	-0.0664	0.0385	0.0570
FC+01514+00075	51301432	87100344	2	3	6	15.1401	0.7501	0.0857	0.1421
FC+01514+00042	51301438	13801133	2	3	6	15.1408	0.4195	0.1484	0.0798
FC+01518+00006	51301435	13801108	2	3	6	15.1825	0.0610	0.0501	0.1852
FC+01533–00034	51301433	13801129	2	3	6	15.3275	-0.3409	0.1338	0.0800
FC+01537+00023	87200204	13801132	6	3	6	15.3704	0.2309	0.1104	0.1006
FC+01542–00073	51301439	87100345	2	3	6	15.4212	-0.7311	0.0992	0.0802
FC+01694+00081	86900607	86900608	6	9	6	16.9399	0.8106	0.1991	0.2268
FC+01829+00005	47200445	13801538	2	3	6	18.2897	0.0453	0.0865	0.0772
FC+01837–00072	47200348	87100547	2	3	6	18.3721	-0.7184	0.0868	0.1436
FC+01857–00021	47200341	13801534	2	3	6	18.5695	-0.2083	0.0609	0.1022
FC+01857+00036	47200444	13801637	2	3	6	18.5830	0.3536	0.0749	0.1323
FC+01861+00011	47200343	13801636	2	3	6	18.6112	0.1117	0.1496	0.1022
FC+01864+00074	47200440	87100546	2	3	6	18.6515	0.7413	0.0882	0.1433
FC+01880–00012	87100406	13801635	2	3	6	18.8094	-0.1247	0.0374	0.1298
FC+01917+00026	47200447	13801562	2	3	6	19.1696	0.2562	0.0473	0.2434
FC+02183+00000	31900455	13801440	6	3	6	21.8287	-0.0016	0.0854	0.1634
FC+02200+00080	47200749	86900948	2	3	6	21.9999	0.8001	0.0858	0.1423
FC+02214–00035	31900351	13801439	2	3	6	22.1388	-0.3499	0.1236	0.1429
FC+02216+00027	47200750	13801741	2	3	6	22.1527	0.2722	0.0748	0.2266
FC+02243+00008	47200751	13801742	2	3	6	22.4331	0.0824	0.0762	0.0509
FC+02556+00008	48100556	13801947	2	3	6	25.5641	0.0806	0.0604	0.0518
FC+02562–00030	48100554	13801945	2	3	6	25.6205	-0.2994	0.0734	0.1230
FC+02567+00046	48100558	13801949	2	3	6	25.6769	0.4595	0.2017	0.0376
FC+02577+00017	87300311	87300312	6	9	6	25.7698	0.1694	0.0992	0.1228
FC+02590–00031	47201155	13801846	2	3	6	25.8989	-0.3089	0.0617	0.1850
FC+02596+00030	48100557	13801848	2	3	6	25.9607	0.3005	0.0731	0.2058
FC+02865+00000	85600913	85600914	6	9	6	28.6510	0.0017	0.1128	0.1437
FC+02990+00034	48000465	13901253	2	3	6	29.9004	0.3362	0.0807	0.1815
FC+02994–00035	48000461	13901250	2	3	6	29.9415	-0.3498	0.1616	0.1636
FC+03028–00074	35000591	85600639	2	3	6	30.2796	-0.7414	0.0608	0.2479
FC+03030–00023	85600717	85600718	6	9	6	30.2981	-0.2300	0.1379	0.1438

Table A-3: Catalogue of ISOGAL FC fields (continued)

Field name	ISO 7 μm obs. num.	ISO 15 μm obs. num.	7 μm filter	15 μm filter	Pixel size (")	l_0 (°)	b_0 (°)	dl (°)	db (°)
FC+03033+00070	35000590	85600638	2	3	6	30.3310	0.7000	0.0732	0.2690
FC+03037+00019	48000466	13901354	2	3	6	30.3732	0.1902	0.0532	0.1023
FC+03097+00020	85600315	85600316	6	9	6	30.9690	0.1996	0.2070	0.1361
FC+03100+00040	48000564	48000562	2	3	6	30.9987	0.3944	0.0888	0.0495
FC+03676–00076	48002271	71900102	2	3	6	36.7622	-0.7581	0.0871	0.1433
FC+03686+00073	48002268	71900101	2	3	6	36.8623	0.7317	0.0873	0.1436
FC+03700+00022	48002269	48002270	2	3	6	37.0006	0.2203	0.1520	0.1220
FC+04495–00075	48300276	72101804	2	3	6	44.9489	-0.7498	0.0856	0.1416
FC+04499+00073	48300172	72101803	2	3	6	44.9875	0.7312	0.0853	0.1427
FC+04499–00021	48300173	13900956	2	3	6	44.9889	-0.2093	0.1620	0.2878
FC+04499+00035	48300274	13901157	2	3	6	44.9891	0.3511	0.1623	0.1628
FC+04526–00032	48300175	13901159	2	3	6	45.2552	-0.3191	0.0964	0.1216
FC+04862+00022	72101743	72101744	6	9	6	48.6213	0.2200	0.1249	0.1440
FC+04911–00070	72500849	72400950	6	9	6	49.1115	-0.7000	0.2858	0.1429
FC+05153+00005	52501878	52501879	2	3	6	51.5292	0.0512	0.1230	0.2271
FC+05195–00075	52501880	72500406	2	3	6	51.9498	-0.7484	0.0846	0.1429
FC+05199+00077	52501877	72500405	2	3	6	51.9889	0.7724	0.0866	0.1429
FC+05318+00014	72500345	72500346	5	9	6	53.1820	0.1302	0.1167	0.1130
FC+05946+00010	52501982	52501983	2	3	6	59.4599	0.1008	0.0952	0.2683
FC+05998–00073	52501984	72500508	2	3	6	59.9785	-0.7276	0.0844	0.1413
FC+06009+00073	52501981	72500507	2	3	6	60.0896	0.7314	0.0822	0.1416
FC+06750+00000	73300137	72102434	2	3	6	67.5005	-0.0025	0.1245	0.2049
FC+06770–00070	73300138	72102435	2	3	6	67.6996	-0.7016	0.0862	0.1421
FC+07506+00069	73300230	73300327	2	3	6	75.0598	0.6904	0.0868	0.1429
FC+07506+00006	73300231	73300328	2	3	6	75.0702	0.0593	0.1244	0.2051
FC+07512–00072	73300232	73300329	2	3	6	75.1197	-0.7193	0.0872	0.1431
FC+08997–00076	73301026	73300823	2	3	6	89.9716	-0.7594	0.0896	0.1432
FC+09000+00077	73301024	73300821	2	3	6	90.0016	0.7705	0.0891	0.1429
FC+09000+00000	73301025	73300822	2	3	6	90.0023	-0.0001	0.1260	0.2050
FC+09748+00072	73300618	73300715	2	3	6	97.4813	0.7208	0.0836	0.1444
FC+09750+00000	73300619	73300716	2	3	6	97.5043	-0.0000	0.1247	0.2056
FC+09766–00070	73300620	73300717	2	3	6	97.6637	-0.6995	0.0870	0.1430
FC+10500+00000	74501513	74501410	2	3	6	104.9997	-0.0000	0.1209	0.2074
FC+10501–00077	74501514	74501411	2	3	6	105.0142	-0.7692	0.0881	0.1443
FC+10505+00071	74501512	74501409	2	3	6	105.0535	0.7108	0.0876	0.1442
FC+10562+00034	79500901	79500902	6	9	6	105.6334	0.3410	0.1382	0.1425
FC+10694+00518	79500811	79500812	6	9	6	106.9432	5.1795	0.0966	0.2043
FC+10886–00100	78800403	78800404	6	9	6	108.8552	-0.9974	0.1325	0.1409
FC+11011–00005	77901505	77901506	6	9	6	110.1079	0.0518	0.1360	0.1430
FC+13376+00100	78801013	78801014	6	9	6	133.7615	1.0011	0.1398	0.1423
FC+13586–00055	81101521	81101522	2	3	6	135.8633	-0.5479	0.0994	0.1022
FC+13825+00160	83901309	83901310	6	9	6	138.2450	1.6008	0.1321	0.1210